Seasonal and inter-annual variability in wetland methane emissions simulated by CLM4Me′ and CAM-Chem and comparisons to observations of concentrations

Lei Meng[1], Rajendra Paudel[2], Peter G. M. Hess[2,] Natalie M. Mahowald[3]

1. Department of Geography and Environmental and Sustainability Studies Program, Western Michigan University, Kalamazoo, MI 49008
2. Department of Earth and Atmospheric Sciences, Cornell University, Ithaca, NY 14850
3. Department of Biological and Environmental Engineering, Cornell University, Ithaca, NY 14850

Manuscript submitted to Biogeosciences on December 11, 2014

Abstract

Understanding the temporal and spatial variation of wetland methane emissions is essential to the estimation of the global methane budget. Our goal for this study is three-fold: (i) to evaluate the wetland methane fluxes simulated in two versions of the Community Land Model, the Carbon-Nitrogen (CN, i.e. CLM4.0) and the Biogeochemistry (BGC, i.e. CLM4.5) versions using the methane emission model CLM4Me′ so as to determine the sensitivity of the emissions to the underlying carbon model; (ii) to compare the simulated atmospheric methane concentrations to observations, including latitudinal gradients and interannual variability so as to determine the extent to which the atmospheric observations constrain the emissions; (iii) to understand the drivers of seasonal and interannual variability in atmospheric wetland methane fluxes. Simulations of the transport and removal of methane use the Community Atmosphere Model (CAM-chem) model in conjunction with CLM4Me′ methane emissions from both CN and BGC simulations and other methane emission sources from literature. In each case we compare model simulated atmospheric methane concentration with observations. In addition, we simulate the atmospheric concentrations based on the TransCom wetland and rice paddy emissions derived from a different terrestrial ecosystem model VISIT. Our analysis indicates CN wetland methane emissions are higher in tropics and lower in high latitudes than emissions from BGC. In CN, methane emissions decrease from 1993 to 2004 while this trend does not appear in the BGC version. In the CN version, methane emission variations follow satellite-derived inundation wetlands closely. However, they are dissimilar in BGC due to its different carbon cycle. CAM-chem model simulations with CLM4Me′ methane emissions suggest

that both prescribed anthropogenic and predicted wetlands methane emissions contribute substantially to seasonal and inter-annual variability in atmospheric methane concentration. Simulated atmospheric CH_4 concentrations in CAM-chem are highly correlated with observations at most of the 14 measurement stations evaluated with an average correlation between 0.71 and 0.80 depending on the simulation (for the period of 1993-2004 for most stations based on data availability). Our results suggest that different spatial patterns of wetland emissions can have significant impacts on N-S atmospheric CH_4 concentration gradients and growth rates. This study suggests that both anthropogenic and wetland emissions have significant contributions to seasonal and inter-annual variations in atmospheric CH_4 concentration. However, our analysis also indicate the existence of large uncertainties in terms of spatial patterns and magnitude of global wetland methane budgets, and that substantial uncertainty comes from the carbon model underlying the methane flux modules.

1. Introduction

The increase in atmospheric methane (CH_4) concentrations since 2007 (Rigby et al., 2008) has received attention due to methane's strong greenhouse effect. The causes of the renewed increase in CH_4 since 2007 and the relative stability of the atmospheric concentrations for the preceding decade (1996-2006) are not well understood (Bloom et al., 2010). Improved understanding of the variability of atmospheric methane can provide more accurate predictions of future concentrations. Changes in atmospheric CH_4 are determined by the balance between the emissions of CH_4 and its loss. The loss is mostly controlled by the reaction of CH_4 with the hydroxyl radical (OH). While the CH_4 loss timescale varies from year to year (Wuebbles and Hayhoe, 2002;Bousquet et al., 2006) as the OH concentration changes, recent evidence suggests the interannual variability of OH is small (Montzka et al., 2011). The primary sources of atmospheric methane include anthropogenic emissions, natural wetlands, rice paddies, biomass burning, and termites (Denman et al., 2007;Kirschke et al., 2013). Natural wetlands are the largest single source of atmospheric CH_4 and make a significant contribution to its variability (Spahni et al., 2011). Using inverse methods Bousquet et al. (2006) suggests that 70% of the global emission anomalies CH_4 for the period 1984-2003 are due to the inter-annual variability in wetland emissions and furthermore that tropical methane emissions are the dominant contribution to the global inter-annual variability. In another methane inversion, Chen and Prinn (2006) find that the large 1998 increase in atmospheric CH_4 concentration could be attributed to global wetland emissions.

There are still large uncertainties in global wetland emissions due to 1) poor understanding of environmental and biological processes that control methane emissions

114 (Riley et al., 2011;Meng et al., 2012); and 2) uncertainties in the extent and distribution
115 of wetlands, particularly in tropical regions (Prigent et al., 2007;Spahni et al., 2011).
116 Process-based biogeochemical methane models can help improve the understanding of
117 dominant processes that control methane production, oxidation, and transport. Several
118 process-based models that incorporate different environmental and biological processes
119 have been developed. For instance, Wania et al. (2009) develop the Wetland Hydrology
120 and Methane (LPJ-WhyMe) model to simulate peatland hydrology and methane
121 emissions from northern latitudes using a mechanistic approach. Recently Spahni et al.
122 (2011) incorporate LPJ-WhyMe into the Lund-Potsdam-Jena dynamic global vegetation
123 model (DGVM) to simulate methane emissions on a global scale by dividing global
124 ecosystems into four different types (northern peatland (45N-90N), naturally inundated
125 wetlands (60S-45N), rice agriculture and wet mineral soils) and using different
126 parameters to characterize the processes relevant for methane production, oxidation, and
127 transport in the soil in each of these ecosystems. Zhuang et al. (2004) couple a methane
128 module to a process-based biogeochemistry model, the Terrestrial Ecosystem Model
129 (TEM), and explicitly calculated methane production, oxidation, and transport in the soil.
130 Xu et al. (2010) include a methane module in the Dynamic Land Ecosystem Model
131 (DLEM) to simulate methane production, oxidation, and transport (Xu et al., 2010). Riley
132 et al. (2011) integrate a methane biogeochemical model (CLM4Me) into the Community
133 Land Model (CLM), the land component of the Community Climate System Models
134 (Gent et al., 2011) and the Community Earth System Model (CESM). Meng et al. (2012)
135 add additional features into CLM4Me including an emission dependence on pH and on
136 redox potential. This revised version of CLM4Me is referred as CLM4Me′ (Meng et al.,

137 2012). Detailed description of CLM4Me and CLM4Me′ can be found in Riley et al.
138 (2011) and Meng et al. (2012). The large uncertainties in methane fluxes due to
139 parameter uncertainty in this model are quantified in Riley et al. (2011).
140 These process-based models are often evaluated against surface CH_4 flux
141 measurements based on chamber techniques (Jauhiainen et al., 2005;Shannon and White,
142 1994;Keller, 1990). However, there are only limited observational datasets available for
143 model evaluation and most of them are in mid- and high latitudes. The shortage of
144 tropical methane measurements makes it difficult to evaluate the spatial distribution of
145 modeled surface emissions. This is especially critical as the tropical wetlands are the
146 largest contribution to global wetland methane emissions (Meng et al., 2012;Spahni et al.,
147 2011;Bloom et al., 2010).
148 The spatial distribution of surface emissions produced by these biogeochemical
149 models can be used along with other CH_4 emission sources as inputs to atmospheric
150 chemistry and transport models to simulate atmospheric CH_4 concentration. As wetland
151 emissions are the largest single source, their spatial distribution could significantly affect
152 the distribution of atmospheric CH_4 concentration. The long-term atmospheric
153 measurement of CH_4 can be used to compare with modeled atmospheric CH_4 to further
154 evaluate the spatial distribution of surface emissions. Recently, a chemistry-transport
155 model (CTM) intercomparison experiment (TransCom-CH_4) quantifies the role of CH_4
156 surface emission distributions in simulating the global distribution of atmospheric
157 methane (Patra et al., 2011). In TransCom-CH_4, twelve chemistry-transport models
158 simulations with different surface emissions are evaluated against measured atmospheric
159 CH_4 concentrations. Patra et al. (2011) find that meteorological conditions and surface

emissions from biomass burning and wetlands can contribute up to 60% of the inter-annual variation (IAV) in the atmospheric CH_4 concentrations. However, in Patra et al. (2011) the methane emissions are specified and do not result from interactions between simulated meteorology and land-carbon models.

In this study, we explore the temporal and spatial variation of wetland methane emissions estimated in the CLM4Me′. The modeled wetland emissions are used with other surface emissions (including emissions from anthropogenic sources, biomass burning, rice paddies, and termites) as inputs to the Community Atmospheric Model with chemistry (CAM-chem). The CH_4 concentration simulated with CAM-chem is compared with a global network of station measurements. The purposes of this paper are 1) to examine seasonal and interannual variations in wetland methane emissions simulated by CLM4Me′ in two different versions of the Community Land Model; 2) **to** compare the simulated atmospheric methane concentrations to observations, including latitudinal gradients and interannual variability so as to determine the extent to which the atmospheric observations constrain the emissions; (iii) to understand the drivers of seasonal and interannual variability in atmospheric methane fluxes. Section 2 describes models, methods and datasets. Results and discussions are presented in section 3. We conclude in section 4 with a summary of major findings.

2. Models and Datasets

2.1 Simulations

Methane emissions from 1993-2004 are simulated and analyzed in four different model configurations (see Table 1). All configurations use Community Atmospheric Model (CAM4) with chemistry (CAM-chem) (Lamarque et al.,

183 2012) to diagnose atmospheric methane. These configurations differ in their
184 specification of methane emissions. Other details of the simulations are identical.
185 The TransCom simulation (Table 1) is reported on as part of the TransCom-CH_4
186 simulations (Patra et al., 2011). The CAM-chem model is one of the twelve models
187 participating in these simulations (Patra et al., 2011). The methane emissions in the
188 TransCom are specified and included the seasonal variation of methane emissions from
189 anthropogenic sources (Olivier and Berdowski, 2001), rice paddies and wetlands (Ito and
190 Inatomi, 2012), biomass burning (van der Werf et al., 2006), and termites (Fung et al.,
191 1991). The wetland emissions from Ito and Inatomi (2012) are calculated based on a
192 process-based terrestrial ecosystem model, the Vegetation Integrative Simulator for Trace
193 gases (VISIT). In the VISIT, the inundated area is calculated based on model-derived
194 rainfall and temperature (Mitchell and Jones, 2005). We select this scenario from the
195 TransCom experiment because it includes the long-term monthly variations of wetland
196 and rice paddy emissions.
197 Differences between the TransCom simulation and the other three simulations
198 analyzed here (see Table 1) include: (1) differences in the specification of the methane
199 emissions from rice paddies and wetlands: in the TransCom simulation the emissions are
200 specified while in the remaining three simulations the methane emissions are obtained
201 from CLM4Me′ a process-based methane biogeochemical model; (2) differences in the
202 specification of fire emissions: in the TransCom simulation fire emissions are taken from
203 Global Fire Emission Database (GFED) version 2 (on average 20 Tg CH_4/yr is emitted)
204 (van der Werf et al., 2006) while in the remaining three simulations the fire emissions are
205 from GFED version 3 (on average 21.1 Tg is CH_4/yr emitted) (Giglio et al., 2010).

206 Two of the configurations analyzed (labeled: CN_a and CN_b) diagnose wetlands
207 and rice paddies methane emissions using CLM4Me′ within the Community Land Model
208 version 4 (CLM4 or CLM-CN) of the Community Earth System Model (CESM); one
209 configuration (labeled BGC) uses CLM4Me′ within the Community Land Model version
210 4.5 (CLM4.5 or CLM-BGC) of the CESM.
211 The wetland emissions simulated by the CLM4Me′ model when integrated in the
212 CLM4.0 (228 Tg/yr) are on the high side of the current estimates (100-284 Tg/yr)
213 (Denman et al., 2007;Kirschke et al., 2013). In order to obtain a reasonable overall
214 methane budget (~517 Tg/yr, within the range of 492-581 Tg/yr shown in Denman et al.
215 (2014) and Kirschke et al. (2013)), we adjust the emissions in the simulations using
216 CLM4.0. In simulation CN_a the anthropogenic emissions used in the TransCom
217 simulations are multiplied by 0.72; in simulation CN_b the wetland emissions are
218 multiplied by 0.64, but the anthropogenic emissions are the same as those in TransCom.
219 Both these rescalings retain the temporal and spatial emission distributions from the
220 original datasets but simulate the approximately correct atmospheric methane
221 concentrations. In the first case (CN_a), where anthropogenic emissions are reduced, the
222 total anthropogenic emissions are 211 Tg/year. This is at the low end of estimated
223 anthropogenic emissions, but within the range (209-273 Tg) report of values in the
224 literature (see IPCC AR4 Chapter 7) (Denman et al., 2007;Kirschke et al., 2013) when
225 excluding biomass burning and rice paddies.
226 On the other hand the wetland emissions simulated by the CLM4Me′ model
227 integrated into CLM4.5 (BGC) are higher than the CLM4.0 (CN) emissions. Therefore,
228 we adjust the wetland emissions in the BGC simulation. In particular in the BGC

simulation the wetland emissions are reduced by 0.74 to match the total methane emissions in the other simulations. Reducing the methane emissions is equivalent to modifying the coefficient for the maximum amount of methane that can be produced from heterotrophic respiration. The reductions used here are within the uncertainties of this estimate (e.g. Riley et al., 2013). The same termite emissions are used in all simulations. The global interannual average of methane emissions used in CN_a, CN_b and BGC are similar to that used in TransCom.

2.2 CLM4Me′.

CLM4Me' (Meng et al., 2012) is a process-based methane biogeochemical models incorporated in the CLM version 4 and CLM version 4.5 of the Community Earth System Model (CESM). The spatial resolution used in this study is 1.8x2.5 degree. CLM4Me' is based on CLM4Me (Riley et al., 2011) and explicitly calculates methane production, methane oxidation, methane ebullition, methane diffusion through soils, and methane transport through aerenchyma. CLM4Me′ is an update of CLM4Me to include a pH and redox functional dependence for methane emissions, and a limitation of aerenchyma in plants in always-inundated areas (Meng et al., 2012). In CLM4Me′, methane production (P (mol C $m^{-2}s^{-1}$)) is calculated as follows:

$$P = R_{\mathrm{H}} f_{\mathrm{CH_4}} Q'_{10} S f_{\mathrm{pH}} f_{\mathrm{pE}}$$

Here, R_{H} is heterotrophic respiration from soil and litter (mol C $m^{-2}s^{-1}$), $f_{\mathrm{CH_4}}$ is the ratio between CO_2 and CH_4 production, which is currently set to 0.2 for wetlands and rice paddies. Q'_{10} is the control of soil temperature on CH_4 production. f_{pH} and f_{pE} are pH and redex potential function, respectively. A detailed description of CLM4Me and CLM4Me′ can be found in Meng et al. (2012) and Riley et al. (2011).

2.3 Community Land Model (CLM)

The CLM4Me′ is integrated and spun up in two versions of the CLM: CLM4.0 and CLM4.5. The CLM4.0 uses the carbon and nitrogen below ground module from the Carbon-Nitrogen (CN) model (Thornton et al., 2007;Thornton et al., 2009). The CLM4.5 is updated from the CLM4.0 and offers some improvements with the most significant change to the below ground carbon cycle (Koven et al., 2013). The CLM4.5 includes an alternate decomposition cascade from the Century soil model, which is referred to as the biogeochemistry version of the model (CLM4.5-BGC). This version of the model has increased productivity and carbon in high latitudes (perhaps an overestimate) and reduced productivity in the tropics compared to the CN model (see Koven et al. (2013) for more comparisons). The initial condition in the both CLM models is created using NCEP-reanalysis datasets in two steps. First the model is brought close to equilibrium for 1850 conditions (atmospheric CO2 concentration, aerosol deposition, nitrogen deposition, and land use change) cycling a 25-year (1948-1972) subset of transient climate data (1948-2004). Then we use these equilibrated conditions in a transient simulation from 1850 to 1990 (where the meteorology is cycled over the period of 1948-2004) to produce the initial condition used in this study. For the period of this study (1990-2005), CLM4Me′ is forced with multi-satellite derived inundation fraction (Prigent et al., 2007) and NCEP (i.e., the National Center for Environmental Prediction) reanalysis datasets (Qian et al., 2006;Kistler et al., 2001). While the simulation period is 1990-2005 satellite inundation data is only available from 1993-2004. We use climatological monthly average (1993-2004) inundation fraction for years 1990-1992 and 2005.

2.4 The CAM-chem model.

We use the CAM-chem (CAM-chem) (Lamarque et al., 2012) is driven by the NCEP reanalysis dataset (Kistler et al., 2001;Qian et al., 2006) to predict the atmospheric concentrations of methane from the methane emissions. In this study, we conduct simulations with CAM-chem using offline meteorological forcing, similar to the model set up used in TransCom (Patra et al., 2011). The simulations are performed at a horizontal resolution of 1.9° (latitude) and 2.5° (longitude) and at 28 vertical layers. Please refer to Lamarque et al. (2012) for a detailed description of CAM-chem.

In the CAM-chem model version used here, the atmospheric chemistry is simplified compared to Lamarque et al. (2012), and includes only the reactions necessary to capture the loss of methane. The simulations include the chemical removal reactions for CH_4 including the reaction with OH, the excited atomic oxygen O1D, and chlorine (Cl). Specifics of the chemical loss reactions can be found in Patra et al. (2011). Interannually constant monthly mean OH is used in the CAM-chem simulations. The optimized OH derived from CH3CCl3 concentrations scaled from Spivakovsky et al. (2000) is used where an equal OH abundance is assumed in both the Northern and Southern Hemispheres. The distribution of OH used to compute the loss of atmospheric methane is identical to that used in TransCom experiments. Stratospheric loss due to Chlorine (Cl) and O1D is also included. Interannually constant monthly Cl and O1D are used in the simulations. In addition a soil sink for CH_4 is included using a climatological monthly average derived from LMDZ atmospheric CH_4 inversion (Bousquet et al., 2006).

295 Atmospheric concentrations of methane are tagged from the rice paddy, wetland,
296 anthropogenic and biomass burning emission sources. The losses of tagged methane are
297 identical to those described above.
298 *2.5 Observed atmospheric CH_4 concentration.*
299 Observational atmospheric CH_4 concentration datasets are obtained from the
300 World Data Centre for Greenhouse Gases (WDCGG) at
301 http://ds.data.jma.go.jp/gmd/wdcgg/. Monthly concentration datasets from 14 stations
302 (Table 2) around the world are compared with the simulated atmospheric CH_4 (Butler et
303 al., 2004;Cunnold et al., 2002). Most of the sites have monthly or weekly measurements
304 and use flask-sampling method. Collected samples are analyzed using gas
305 chromatography with flame ionization detection (Dlugokencky et al., 2005).
306 *2.5 RMS Variability.*
307 Seasonal and inter-annual Root Mean Square (RMS) variability are used to
308 evaluate the spatial distribution of simulated methane variability. We apply the method
309 described in Nevison et al. (2008). Here, seasonal RMS variability is calculated as the
310 RMS of the differences between model climatological monthly means (1990-2004) and
311 the climatological annual mean. The interannual variability of RMS is calculated as the
312 RMS of the differences between each month and the corresponding month from the
313 climatological seasonal cycle. We calculate RMS separately for methane tagged from
314 each tagged emission source. This apportions the variability of each source by calculating
315 the ratio between the variability due to that source's RMS and the total RMS. Please note
316 that the sum of individual source's contribution to total RMS is often greater than 1 in
317 cases of cancelation of signals among individual sources.

318 *2.6 Taylor Diagrams.*

319 Taylor diagrams can provide a concise statistical summary of model performance
320 in a single polar coordinate plot (Taylor, 2001). In this study, we use Taylor diagrams to
321 evaluate the model's ability to simulate the observed inter-annual variability (IAV) of
322 atmospheric CH_4. The Taylor diagram gives the model-measurement coefficient R
323 reflecting the agreement in shape and phasing of the model and measurement time series
324 and the ratio of modeled to measured standard deviation $\sigma_{\text{model}}/\sigma_{\text{obs}}$, which represents
325 the agreement between the amplitude of the simulated and observed inter-annual
326 variability (IAV) of atmospheric CH_4.

327 **3. Results and Discussions**

328 *3.1 Comparison of methane fluxes from different sources*

329 A comparison of methane fluxes used in the four experiments shows that wetlands
330 and rice paddies methane emissions in CN_a are higher than those used in other three
331 simulations (Fig.1). Emissions from wetlands and rice paddies in the CN_b simulation
332 (i.e., the CN_a wetland emissions reduced by 36%) simulations are comparable with
333 those used in TransCom and BGC experiments (Fig.1). There are different magnitudes in
334 the seasonal and inter-annual variations among these four experiments. Overall, BGC has
335 the lowest winter emissions. There is a decreasing trend in the CN_a and CN_b methane
336 emissions not evident in the TransCom and BGC methane emissions. The difference in
337 methane emissions in CN_a, CN_b, and BGC experiments will be discussed in the next
338 session. The fire emissions in the TransCom simulation (based on GFED v2) and the
339 other simulations (based on GFED v3) (Fig. 2) are similar in magnitude, but with some
340 distinct seasonal differences.

341 Overall, the anthropogenic methane emissions tend to stabilize after 1998, due to
342 the decrease from mid- and high latitudes (Fig. 3). The annual total methane emissions
343 used in CN_a and CN_b experiments are slightly higher (lower) than that used in
344 TransCom experiment during the first (second) half of the study period (Fig. 4). The
345 annual total emissions used in BGC are slightly lower than those used in TransCom
346 during most years except 1997,1998, and 2002. There are no statistically significant
347 trends (at ~95% level) in the difference between the BGC and TransCom total emissions.
348 3.2 *Seasonal and inter-annual variability in CN_a and BGC methane emissions.*
349 3.2.1 CN_a methane emissions
350 There are strong seasonal and inter-annual variations in CN_a wetland methane
351 emissions (Fig. 5). On a seasonal basis, the peak methane emissions occur in the summer
352 (June, July, and August) and the lowest methane emissions occur in winter (December,
353 January, February) as methane emission is controlled by both temperatures and inundated
354 area. On an inter-annual basis, the summer of 1994 has the highest CN_a methane
355 emissions methane emissions in the period of 1993-2004. A generally decreasing trend (-
356 2.1 Tg CH_4/year, significant at 95% level) in CN_a global wetland emissions occur from
357 1994 to 2004. This is driven by trends in tropical wetland emissions (Fig. 5), where
358 tropical wetlands contribute to ~70% of the global wetland flux. The decreasing rate in
359 tropical wetland emissions from 1993-2004 is approximately -1.68 Tg CH_4/year,
360 statistically significantly different from 0 (no change) at the 95% confidence level.
361 We further identify the four highest (1994, 1995,1996,1999) and lowest
362 (2001,2002,2003,2004) annual CN_a methane emissions in the period of 1993-2004 and
363 plot the difference of methane emissions between the average of the 4 extreme high and

364 low emission years (Fig. 6A). There are large differences across much of the globe, but
365 the largest difference occurs in the tropics (see the latitudinal average on the right). On a
366 regional level, the largest differences are primarily present in Indonesia and South
367 America (e.g., Amazon regions).

368 *3.2.2 BGC methane emissions*

369 The trend in BGC wetland methane emissions is different from that in CN_a
370 experiment (Fig. 5). In the BGC simulation, the peak emissions occur in 2002 instead of
371 1994. The wetland emissions do not decrease significantly from 1993 to 2004 with no
372 significant trends in the inter-annual methane emissions in the mid- and high- latitudes
373 and the tropics in these simulations. There are several additional differences between
374 CN_a and BGC wetland emissions: 1) global BGC wetland emissions are approximately
375 10% lower than CN_a wetland emissions; 2) the BGC tropical (-30S-20N) wetland
376 emissions of 63 Tg CH4/yr are approximately 60% lower than those in CN_a (158 Tg
377 CH_4/yr); 3) high latitudes (>50N) wetland emissions in BGC are 97 Tg CH_4/yr while
378 CN_a only produces 12 Tg CH_4/yr. Such large differences are probably largely due to the
379 shift of carbon from tropics to high latitudes as a result of the modifications from CN_a
380 to BGC (see section 3.2.3) (Koven et al., 2013). BGC and CN_a produce similar methane
381 emissions in the mid-latitudes (20N-50N).

382 The latitudinal distribution of the methane emissions in CN_a suggests the largest
383 seasonal variation occurs at approximately 20N-30N, followed by the latitudinal band
384 50N-60N (Fig. 7A). High latitudes (>65N) have no clear seasonal cycles due to the low
385 methane fluxes that CN_a produces in the high latitudes (Meng et al. 2012). There is a
386 very dampened seasonal variation of CH_4 emissions in tropical wetlands (10S-10N),

387 although tropical wetlands are the largest contribution to total wetland emissions. The
388 seasonal cycle in the different latitudinal bands is consistent with that identified in Spahni
389 et al. (2011) (see their Fig. 4a).
390 The latitudinal distribution of methane emissions shows a strong seasonal
391 variation in high latitudes in the BGC simulation. As clearly shown in Fig. 7B, peak
392 methane emissions (>200 mg $CH_4/m^2/d$) occur in summer seasons and low methane
393 emissions (~10 mg $CH_4/m^2/d$) are present in winter. The maximum emissions occur at
394 approximately 60N as distinct from the CN_a simulations.
395 The peak emissions in BGC from 1993-2004 occur in 1998 followed by 2002,
396 1994, and 2003. The four lowest emission years are 1999, 2000,2001, and 1996. As
397 shown in Fig. 6B, the increase in methane emissions from the four lowest to highest years
398 is primarily on the equator, in the Southern Hemisphere (around 30S) and in the high
399 latitudes (50N-70N). This is distinct from the CN_a simulations where the largest change
400 predominantly occurs in the tropics (Fig. 6A).
401 3.2.3 Sources of the differences in CLM4.0 and CLM4.5 estimated methane
402 emissions
403 The large difference in spatial distribution of methane emissions between CN_a
404 (CLM4.0) and BGC (CLM4.5) experiment is due to the change in soil biogeochemistry
405 within the soil C and N models from CLM4.0 to CLM4.5. Koven et al. (2013) conduct a
406 detailed analysis of the effect of such changes on C dynamics in the CLM model. Here
407 we briefly describe the changes that most affect high latitudes and tropiccal C dynamics,
408 where the differences are the largest. The carbon cycle is linked to the Nitrogen (N) cycle
409 because N availability in soils will affect vegetation growth. In the CLM4.0, available

410 mineral N experiences a first-order decay with a time constant of two days that is not
411 subject to environmental limitations. In high latitudes, the long winters allow most
412 mineral N to decay and only a limited amount of N is available for vegetative growth
413 during the short growing season. Therefore, in the high latitudes CLM4.0 simulates low
414 productivity and low heterotrophic respiration (HR) available for methane production (in
415 CLM4Me, methane production is a function of heterotrophic respiration, see methane
416 production equation in section 2.1). In CLM4.5, an introduction of the dependence of N
417 losses on temperature and soil moisture and seasonality of N fixation reduce the
418 unrealistic N limitation in CLM4.0. Thus, CLM4.5 allows for more N to be used for
419 vegetation growth and produces higher soil carbon, higher heterotrophic respiration (HR),
420 and thus higher methane fluxes. As shown in Appendix A, HR in CLM4.5 is much higher
421 than that in CLM4.0, particularly in the northern hemisphere summer season when most
422 CH_4 is produced. For Please note that annual CH_4 emissions from northern latitudes are
423 not affected by winter time HR because CH_4 is not produced in winter seasons due to
424 below-freezing temperatures.

425 Other changes that affect tropical C dynamics include calculation of
426 decomposition rates at each model level in CLM4.5 instead of limiting to top 30 cm in
427 CLM4.0 based on moisture and temperatures and inclusion of oxygen availability as a
428 limitation factor as well as vertical mixing of soil organic matters. These changes
429 primarily reduce terrestrial gross primary productivity (GPP) in tropical forests as a result
430 of reduction in photosynthesis. The change in nitrogen cycle described above also has an
431 effect on tropical C dynamics by removing N limitation, which makes the biosphere more
432 sensitive to the increased temperature and CO_2 concentration and leads to a large net

uptake of carbon. The overall effect of the changes in CLM4.5 in the tropics is to reduce heterotrophic respiration (HR), resulting in a decrease in methane production. Appendix A shows the HR is much lower in CLM4.5 compared to CLM4.0 in the tropics. Comparisons of NPP and Soil C between CLM4.5 and CLM4.0 are presented in Appendix B and C.

3.3 Contribution of individual sources to seasonal and inter-annual variability in atmospheric CH_4.

In order to determine the relative contribution of each source to total atmospheric CH_4 variability as simulated in CAM-Chem model, we calculate the seasonal and inter-annual Root Mean Square (RMS) variability for the total CH_4 concentration and the partial contribution of the anthropogenic source, rice paddies, and wetlands to the overall RMS (Figs. 8 and 9). These three sources have the largest contribution to the annual RMS due to their large magnitudes.

3.3.1 Seasonal and inter-annual variability in CN_a methane emissions

Seasonal variability of atmospheric methane concentration is high in the tropics and southern Hemisphere and low in the northern high latitudes in the CN_a simulations (Fig. 8). The low seasonal variability in the northern high latitudes is consistent with the relatively low magnitude of northern high latitude methane fluxes in the CN_a simulations, plus the fact that the highest emissions occur during the summer, when the vertical mixing is highest.

Inter-annual variability (IAV) in RMS is relatively homogeneous across the globe with slightly higher IAV in the southern hemisphere (Fig. 8). Overall the IAV RMS of atmospheric methane is generally larger than the seasonal RMS. Both anthropogenic

456 sources and wetlands are the dominant contributors to the seasonal RMS variability in the
457 northern hemisphere (Fig. 8), while wetlands are the only dominant contributor to the
458 IAV RMS variability. This is in agreement with Bousquet et al. (2006) that wetland
459 emissions dominate the inter-annual variability of methane sources. Rice paddies play a
460 more important role in seasonal RMS variability than in inter-annual RMS variability
461 over Asia and North America. This is consistent with the largest seasonal variations in
462 rice paddy emissions occur over Asia and North America (Meng et al. 2013). Similar
463 results are also found in CN_b simulations.

464 3.3.2 Seasonal and inter-annual variability in BGC methane emissions

465 Compared to CN_a, the BGC methane emissions show higher seasonal and inter-
466 annual variability, particularly in high-latitudes (Fig. 9). For instance, Alaska and Siberia
467 are two regions that have the highest variability. For both the seasonal and inter-annual
468 variations, wetlands dominate the variability, followed by anthropogenic sources. Rice
469 paddies only play a role in the tropics (0-30N). Both wetlands and anthropogenic
470 methane emissions in BGC contribute a higher percentage to the inter-annual variations
471 than in the CN_a simulations.

472 *3.4 Interhemispheric gradients in atmospheric CH_4 concentrations*
473
474 The latitudinal gradient from TransCom, CN_a, CN_b, BGC, and observations is
475 shown in Fig. 10. The latitudinal gradient is defined as the difference in averaged CH_4
476 concentration between Northern and Southern Hemispheres (N-S gradients) stations
477 listed in Table 2. The N-S gradients produced in all four simulations are highly correlated
478 with observations for the period of 1993-2004 (Fig. 10). The correlations (r) are
479 0.83,0.72, 0.76, 0.91 (all four correlations are significant at 95% confidence level) for

480 TransCom, CN_a, CN_b, and BGC, respectively. It is also clearly shown in Fig. 10 that
481 the TransCom and CN_a simulations underestimate the N-S hemisphere gradients. The
482 underestimation of N-S gradients in CN_a might be due to the high tropical wetland
483 emissions in this case as the high tropical emissions are likely to increase the CH4
484 concentration in the Southern Hemisphere. The BGC simulation significantly
485 overestimates the N-S hemisphere gradients, by about 70%, consistent with the large high
486 latitude methane emissions in this simulation and the low tropical emissions. The CN_b
487 simulation, with the same anthropogenic emissions as TransCom, but decreased wetland
488 methane emissions compared with CN_a best reproduces the observed N-S gradient
489 during the period of 1993-2004. The N-S gradients decrease between 1993 and 2004 in
490 TransCom, CN_a, and CN_b experiments, although there is only slight decrease in the
491 measurements (Fig. 10). Dlugokencky et al. (2011) calculate the inter-polar difference
492 (IPD) (difference between northern (53N-90N) and southern (53S-90S) annual mean CH_4
493 concentration) from the observations and find a slight decrease in IPD from 1993 to
494 2010.

495 *3.5 Evaluation of model inter-annual variability*
496
497 Model simulation of the IAV of atmospheric CH_4 concentration is evaluated
498 against site observations over 14 stations (Table 1) around the world. The climatological
499 seasonal cycle is removed in order to focus on the IAV. CN_a simulates the trend in
500 methane from 1993 to approximately 2001 at all of the stations, but tends to
501 underestimate observations during the later period (2001-2004) (Fig. 11). Such an
502 underestimation might be due to the large decrease in CN_a simulated wetland emissions
503 (Fig. 5). The CN_b simulation with decreased wetland emissions (CN_b in Fig. 11)

shows increased atmospheric methane concentrations during the later period (2001-2004) allowing for a better match between observations and model simulations. In the BGC simulation, model simulated atmospheric concentrations are relatively flat from 1998 to 2004, which match the observations well (Fig. 11). In the TransCom experiment, simulated CH_4 concentration anomalies are generally in good agreement with observations at all of the stations.

The Taylor diagram of model-observation comparisons of interannual variability show that TransCom performed the best among the three cases while CN_b and BGC simulations performed slightly better than CN_a due to a better correlation with the measurements (Fig. 12). The performance of BGC simulations is comparable to (or slightly better than) TransCom in terms of the correlation (Fig. 13) although the model tends to overpredict the amplitude of the inter-annual variability. Decreasing wetland emissions (CN_b) allows for a better match between model simulations and observations. This suggests that CN_a simulations might overestimate wetland emissions, which agrees with the findings in Kirschke et al. (2013).

3.6 Methane growth rate

The growth rate refers to the average increase in atmospheric CH_4 concentration per year. We calculate the growth rate at each station from the observations and for each simulation. The observed average growth rate ranges from 3.2 to 4.6 ppb/yr with an average of 4.0 ppb/yr (Fig. 14, Table 3). The average growth rate in TransCom, CN_a, CN_b, and BGC experiments is 4.2 ppb/yr, 3.29/yr, 4.05 ppb/yr, and 5.68 ppb/yr, respectively (Table 3). The growth rate in TransCom, CN_a, CN_b and BGC simulations has a large range (from -0.48 ppb/yr to 6.44 ppb/yr) at all stations analyzed. As can be

528 seen from Fig. 14, both CN_a and CN_b tend to underestimate the observed growth rate
529 in the Northern Hemisphere, but overestimate it in the Southern Hemisphere (Fig. 14)
530 except for the South Pole station. BGC tends to overestimate growth rate in the Northern
531 Hemisphere, particularly in the high latitudes (Fig. 14). TransCom gives better agreement
532 with the measured growth rates in the southern Hemisphere than in the northern
533 Hemisphere. The largest difference in the growth rate between the three cases and the
534 observations occur at the Zeppelinfjellet (zep, Norway) where the average growth rate in
535 TransCom, CN_a, CN_b, BGC and observations was -0.92 ppb/yr, -0.48 ppb/yr, 1.99
536 ppb/yr, 4.2 ppb/yr, and 3.4 ppb/yr, respectively (Table 3). The largest difference between
537 BGC and observations is at Barrow, where the growth rate in BGC experiment was
538 approximately 2 times of that in observations. Overall, CN_a and CN_b underestimate
539 the station growth rate in high latitudes while BGC overestimates it.

540 In addition, a summary of the comparison of model N-S gradients, annual growth
541 rates, and inter-annual variability with observations is presented in Fig. 15. Four stations
542 are specifically selected to represent the South Pole, tropical region, mid-latitudes, and
543 high northern latitudes. Root mean square errors and biases for the four simulations at
544 these four stations are listed in Table 4. As seen in Fig.15, and discussed above, no one
545 model simulation best matches all the observational metrics.

546 3.7 Comparison of inter-annual variability between this study and others

547 We also compare the inter-annual variability in CH_4 emission anomalies in the
548 simulations analyzed here with those given in Spahni et al. (2011), in an updated long
549 term atmospheric synthesis inversion from Bousquet et al. (2006) and from Ringeval et al.
550 (2010) (Fig. 16). As discussed above, the CN_a emissions reach their maximum in 1994

551 and decrease thereafter from 1994-2004 (Fig. 16). The BGC emissions have the highest
552 emissions in 1998 followed by the lowest emissions in 1999 followed by increased
553 emissions from 1999 to 2004. The TransCom emissions increase from 1993 to 1998 and
554 slightly decrease thereafter. The wetland emissions in Ringeval et al. (2010) decrease
555 from 1993-2000. The Ringeval et al. (2010) averaged annual wetland methane emissions
556 are ~215 Tg/yr, similar to the CN_a wetland emissions. However, the atmospheric
557 synthesis inversions of global wetlands (update of Bousquet et al. 2006 (constant OH))
558 wetland emissions increase from 1990 to 2000 followed by a decrease from 2000 to 2005.
559 Thus there seems to be little agreement in the interannual variability of the wetland
560 methane emissions between these various simulations.

561 We further compare our model-derived wetland emissions with those from
562 Wetland Model Inter-comparison of Models Project (WETCHIMP) (Melton et al.,
563 2013;Wania et al., 2013). We conduct two different comparisons: one comparison
564 includes all models with their different parameterizations of wetland extent while the
565 other focuses on models that are driven by satellite inundation datasets (see Table 1,
566 Melton et al., 2013).

567 Each model analyzed in Melton et al. (2013) uses a different wetland
568 parameterization to estimate their wetland extent (See Table 1 in Melton et al. 2013 for
569 details). Therefore, it is not surprising to see the large variation in the wetland extent
570 among all these models from 1993-2004 (Fig. 17). Amongst the models analyzed in
571 Melton et al. (2013) only the LPJ-WSL model uses a prescribed monthly inundation
572 datasets, similar to our simulations (Fig. 17). DLEM_norice prescribes maximum extent
573 at each gridcell from satellite inundation datasets but with simulated intra-annual

574 dynamics. All the simulations making use of the satellite measurements (this study, LPJ-
575 WSL, BGC, and DLEM_norice) show a decrease in wetland extent from 1993-2004. The
576 wetland extent anomalies in DLEM_norice simulations differ as the intra-annual
577 dynamics are simulated (Fig. 17).

578 The models that do not use a prescribed satellite inundation dataset do not
579 simulate notable decreases in wetland extent during the period of 1993-2004 (Fig. 17).
580 This is not in agreement with the satellite inundation dataset: Papa et al. (2010) find ~5.7%
581 decrease in mean annual maximum inundation from 1993 to 2004 with maximum
582 decrease in the tropics (see appendix). In fact, all models (excluding LPJ-WSL,
583 DLEM_norice, and this study) show large increases in wetland extent in 1998 compared
584 to that in 1997, which is also documented in Melton et al. (2013).

585 Melton et al. (2013) demonstrate that the difference in wetland area used in
586 different models might partially explain the discrepancy in model estimated wetland
587 emissions. As shown in Melton et al. (2013), model-derived methane emissions are
588 strongly correlated with the wetland extent (with an average correlation of 0.90 on the
589 global scale). All models that produce a peak methane emission in 1998 have a maximum
590 wetland extent at the same time (Fig. 18). The difference in model-derived methane
591 emission can be attributed partially to the different wetland area used in each model,
592 where the wetland extent is highly uncertain (Melton et al., 2013). However, it should be
593 noted that there are several limitations associated with using wetland extent derived from
594 satellite inundation datasets. As suggested in Prigent et al. (2007), satellites might
595 underestimate inundated areas due to their incapability to detect small water bodies.
596 Further, satellite datasets only include fully inundated area and excluded unsaturated wet

597 mineral soils, which might also be important wetland methane source (Spahni et al.,
598 2011).

599 The methane emission anomalies in DLEM_norice and LPJ_WSL (the
600 simulations in Melton et al. (2013) using satellite or satellite derived wetland extent)
601 show similar temporal variations, as do the methane anomalies in CN_a and CN_b
602 simulations (Fig. 18). Emissions estimated in CN_a, CN_b, DLEM_norice, and
603 LPJ_WSL peak in 1993-1994 and decrease since then. Such a decreasing trend is
604 consistent with the decrease in wetland extent used in these models (Fig. 17). The CN_a
605 and CN_b simulations show a large increase in emissions from 1993 to 1994, but do not
606 simulate large increases in methane emissions from 2001 to 2002 even though wetland
607 extent increases during this period. It should be noted that the BGC simulation uses the
608 same wetland extent as CN_a and CN_b but does not give the same large decrease in the
609 emissions during the period of 1993-2004. In fact, the BGC model gives decreasing
610 emissions from 1993-1994 but increasing methane emissions from 2001-2002. The BGC
611 model also shows that the highest emission occurs in 1998 and the lowest in 1999 during
612 the period of 1993-2004.

613 Both the large increase in the methane emissions from 1993 to 1994 in CN_a and
614 CN_b and the small increase from 2001 to 2002 are likely due to the changes in
615 heterotrophic respiration (HR) in CN_a simulations (Fig. 19). Please note that the
616 methane production in the models is a function of HR (see the methane production
617 equation in section 2.1). Please see Meng et al. (2012) and Riley et al. (2011) for the
618 detailed description of the processes on methane production, oxidation, and transport).
619 HR increases dramatically in CN_a from 1993 to 1994 (Fig. 19) driving higher methane

emissions whereas the decrease in HR from 2001 to 2002 decreases wetland methane production, which might offset the increase in methane emissions from wetland extent. The HR in the BGC simulation is rather different, consistent with the different behavior between CN_a and CN_b and the BGC simulations. Zhao et al. (2005) estimate the net primary production (NPP) from satellites and found that NPP in 2001 is higher than those in 2002 and 2003. Please note that NPP is related to HR. The correlation of global wetland emissions with HR and wetland extent is 0.81 and 0.94, respectively, in CN_a simulations. In BGC simulations, simulated global wetland emissions are also highly correlated with HR (0.89) and with wetland extent (0.81), respectively. Such high correlations suggest that both HR and wetland extent are dominate drivers of wetland methane emissions in CN_a and BGC models. Thus, although BGC experiment uses the same satellite inundated area in CN_a, it does not produce a decreasing trend in methane emissions during the period, probably due to its different trend in HR estimated in BGC as compared with that in CN_a (Fig. 19).

4 Conclusions

In this study, we evaluate the temporal and spatial patterns in wetland methane emissions simulated in the CLM4Me' from two different parameterizations of soil carbon-nitrogen dynamics as included in the CLM4.0 (CN_a and CN_b) and CLM4.5 (BGC). The subsequent methane distributions are simulated in CAM-chem using meteorological drivers consistent with those used to drive the CN and BGC models. Our goals for this study are to: (i) to evaluate the wetland methane fluxes simulated in the two versions of the CLM **so as determine the sensitivity of methane emissions to the underlying carbon model; (ii) to** compare the simulated atmospheric methane

643 concentrations to atmospheric measurements, including latitudinal gradients and
644 interannual variability so as to determine the extent to which the atmospheric
645 observations constrain the emissions; (iii) to understand the drivers of seasonal and
646 interannual variability in atmospheric methane fluxes.

647 Even though driven by identical meteorological forcing and satellite derived
648 wetland area there are significant differences in the interannual and spatial variations
649 between the CN and BGC wetland methane emissions as derived by CLM4Me'. This
650 demonstrates the critical sensitivity in the simulation of wetland emissions to the
651 underlying model. Compared to the CN_a simulations, the BGC simulations produce
652 large emissions (~97 Tg/yr on average) in the northern high latitudes (50N-90N) with
653 very strong seasonal variations (from no emissions in NH winter to more than 300 Tg/yr
654 in NH summer) and relatively small wetland emissions (only ~30% of global wetland
655 emissions) in the tropical region. On the otherhand the CN_a simulation has very large
656 tropical emissions (~70% of global wetland emissions) so that changes in the tropics
657 dominate the global emissions.

658 The large difference in their high latitude emissions can be ascribed to the
659 different simulation of nitrogen dynamics in the CN and BGC simulations. In the
660 CLM4.0, available mineral N experiences a first-order decay with a time constant of two
661 days that is not subject to environmental limitations while in the BGC simulation the an
662 introduction of the dependence of N losses on temperature and soil moisture and
663 seasonality of N fixation reduce the unrealistic N loss in CLM4.0. The larger nitrogen
664 availability in the BGC model in high latitudes allows greater carbon pools to develop
665 thus increasing the heterotrophic respiration in high latitudes. The large difference in

tropical wetland emissions between the BGC and CN_a experiments is possibly due to the changes in decomposition rates, carbon vertical mixing, and the release of nitrogen limitation from the CN_a to the BGC model (Koven et al. 2013). Overall these changes reduce NPP and HR in the tropic, which directly impacts the methane fluxes.

Both the CN and BGC simulations also differ in the relative magnitude of seasonal vs. inter-annual variability (IAV) of atmospheric methane concentrations for the period of 1993-2004. IAV is relatively higher (Average total RMS is approximately 20 ppb) than the seasonal variability (approximately 10 ppb) across the globe in CN_a (Fig. 8), while in BGC, IAV is much higher (~25 ppb) than the seasonal variability (~10 ppb) except for the northern latitudes (>50N) (Fig. 9). Both anthropogenic sources and wetlands contribute significantly to seasonal variations of atmospheric methane concentrations in CN_a and BGC. On the inter-annual scale, wetland emissions dominate the global inter-annual variability when CAM-chem is forced with either the CN_a or BGC methane emissions, in agreement with findings in Bousquet et al. (2006).

There are also substantial differences in the interannual variability between the two model versions. CN_a wetland emissions suggest a decreasing trend from 1994 to 2004, which is similar to those estimates from Ringeval et al. (2010) and DLEM_norice and LPJ-WSL models (Melton et al., 2013;Wania et al., 2013). On the other hand, CLM4Me' methane emissions driven by CLM4.5 (the BGC simulation) are highest in 1999 and do not show the significant decrease during the period. The updated estimate from Bousquet et al. (2006) gives increasing emissions from 1991-2000 and a decrease after 2000. A few participating wetland emission models in the WETCHIMP project also predict a peak methane emission in the middle of the period (around 1998-1999).

689 The methane emissions in all simulations conducted here are input into CAM-
690 chem so as to constrain the resulting atmospheric methane concentrations against
691 atmospheric measurements. The meteorological fields driving the atmospheric and the
692 land models are consistent. In particular we compare the simulations against measured
693 interhemispheric gradient, the interannual variability, and the growth rate. Our results
694 show that CN_b simulations (with reduced CN_a wetland emissions) is able to better
695 produce observed atmospheric methane concentrations and observed N-S gradient in
696 methane concentrations, suggesting that CN_a might overestimate the current wetland
697 emissions. In the BGC experiment, modeled atmospheric interannual variability in
698 concentrations has higher correlations with observations than CN_a and CN_b
699 simulations in the majority of stations (Fig. 13). In the TransCom experiment, the
700 magnitude of the correlation between modeled atmospheric concentrations and
701 observations is similar to that of the BGC experiment. We also find that CN_b
702 experiments tend to underestimate the growth rate and BGC overestimates it in high
703 latitudes. TransCom simulations have an overall better estimation of the growth rate at all
704 stations than the other three simulations. In terms of the N-S gradients, CN_b
705 experiments have the closest match with observations among all experiments. BGC
706 overestimated the N-S gradients by ~70% while CN_a and TransCom underestimate it by
707 ~10% and ~20%, respectively. Note that BGC predicts much higher methane emissions
708 from the high latitudes (>50N) than CN_a and CN_b experiments. These simulations
709 generally suggest that the BGC high latitude fluxes (~97 Tg/yr) are unlikely due to its
710 overestimation of the N-S gradients by ~70%. The high latitude methane emissions
711 should be somewhere in the broad range between those used in CN_b (~7.7 Tg/yr) and

712 BGC (~97 Tg/yr). In general, however, no one model simulation best matches all the
713 observational metrics. This study confirms that the large variation in methane emissions
714 exists and wetland methane emissions play an important role in affecting atmospheric
715 methane concentration (Bousquet et al., 2006).
716
717 The comparison of the IAV demonstrates large disagreement between different estimates
718 of the annual wetland emissions. Such a discrepancy in the variability produced in
719 different models suggests that wetland extent plays an important role in controlling
720 wetland emissions. We find large uncertainties exist in wetland extent and wetland
721 methane emissions, in support of the conclusions from Melton et al. (2013). For instance,
722 all models (excluding DLEM_norice and LPJ-WSL) that estimate a peak methane
723 emission in 1998 also produce a peak wetland extent during the same period of 1993-
724 2004. Such a decrease after 2003 is consistent with a decrease in the tropical inundated
725 area, based on satellite observations.
726 In addition to wetland extent, the model simulated carbon pool also has a
727 significant impact on methane emissions (Riley et al., 2011;Bloom et al., 2012). Both
728 CN_a and BGC methane simulations are forced with the same satellite inundated
729 fraction, they produce large differences in both spatial and temporal variations of
730 methane emissions due to the fact that CN_a and BGC use different carbon cycle models.
731 Although satellite inundated area increased from 2001 to 2002, CN_a estimates small
732 increases in methane emissions from 2001 to 2002 due to decreases in HR. BGC
733 produces different methane emissions in terms of spatial and temporal trends, probably

due to the shift of carbon uptake and release from tropics to northern high latitudes as a result of multi-level biogeochemistry in BGC (Koven et al., 2013).

This study suggests that model estimated methane budget is sensitive not only to wetland extent (Melton et al., 2013), but also to the details of the carbon model from which methane fluxes are estimated. Accurate simulations of both are necessary to simulate the interannual variation in wetland methane emissions. Further research should focus on regional wetlands (such as high-latitude and tropical wetlands) in order to have a better estimate of wetland methane budget and its spatial variation.

Appendix A

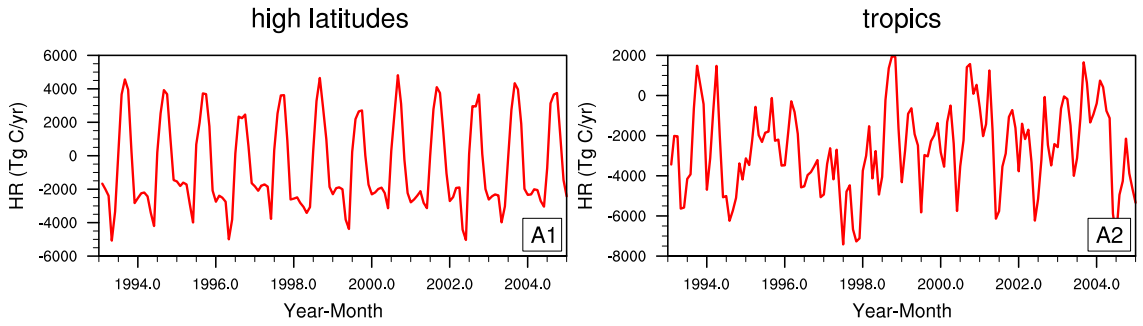

Fig. A Temporal variation of the difference in HR between CLM4.5 (BGC) and CLM4.0 (CN_a) simulations (CLM4.5 minus CLM4.0) in high latitudes (Fig. A1) and in tropical regions (Fig. A2). We use units TgC/yr so that it can be easily compared with Fig. 5.

Appendix B

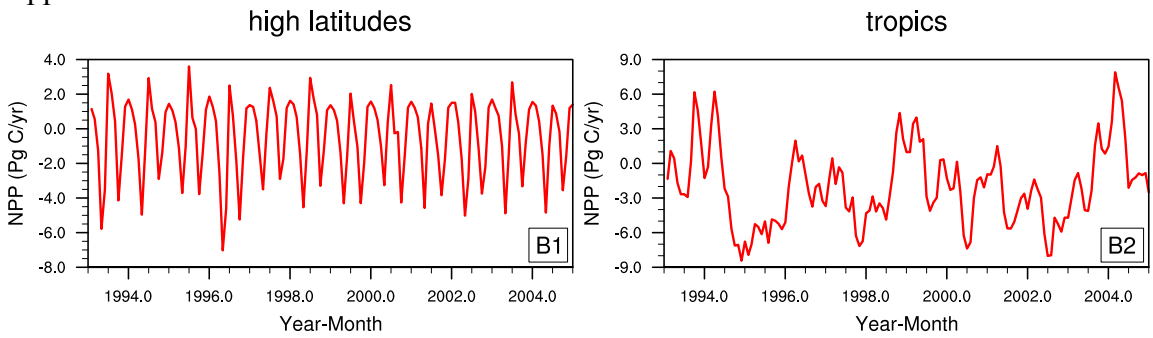

Fig. B Temporal variation of the difference in NPP between CLM4.5 (BGC) and CLM4.0 (CN_a) simulations (CLM4.5 minus CLM4.0) in high latitudes (B1) and tropics (B2).

Appendix C

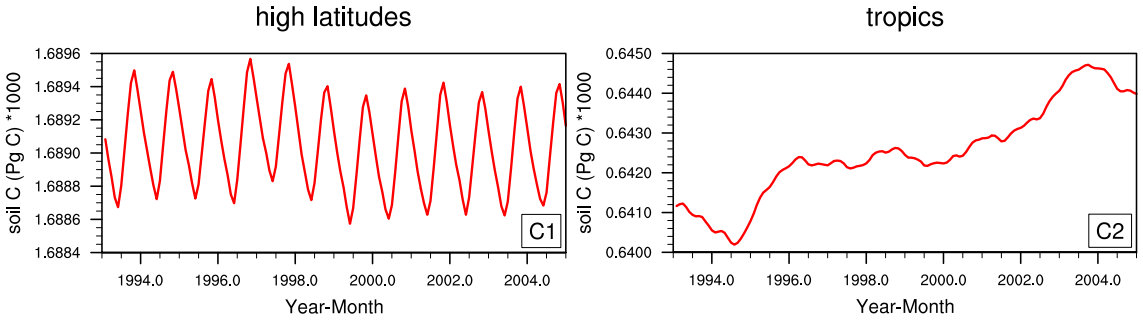

Fig. C Temporal variation of the difference in soil C between CLM4.5 (BGC) and CLM4.0 (CN_a) simulations (CLM4.5 minus CLM4.0) in high latitudes (C1) and tropics

(B2). Please note that the CN_a model produced substantially less soil C than the BGC model. In addition, CN_a produced more soil C in tropics than in high latitudes while BGC produced more soil C in high latitudes than in tropics. This result is consistent with Koven et al. (2013). These differences are due to changes in vegetation productivity as a result of soil N feedback from the revised denitrification in the BGC model.

Acknowledgements

The authors would like to thank Dr. Joe Melton for providing model datasets from the Wetland and Wetland CH4 Inter-comparison of Models Project (WETCHIMP). Part of the work was supported by NASA grant DE-SC0006791.

Table 1 Comparison of the methane sources in the four simulations used in this study.

Input Data	TransCom	CN_a	CN_b	BGC
Anthropogenic Emissions	OB2001[1]	0.72*OB2001	OB2001	OB2001
Wetland emissions	Ito and Inatomi, 2012[5]	CLM4.0[2]	0.64*CLM4.0[2]	0.74*CLM4.5[3]
Rice paddy emissions	Ito and Inatomi, 2012	CLM4.0	CLM4.0	CLM4.5
Termite emissions	Fung et al. 1991	Fung et al. 1991	Fung et al. 1991	Fung et al. 1991
Fire emissions	GFED v2[4]	GFED v3	GFED v3	GFED v3

[1]OB2001 refers to the anthropogenic methane emissions in Olivier and Berdowski (2001). The average annual CH4 emissions are ~294 Tg/year over the period of 1993-2004.

[2] CLM4.0 refers to the methane emissions estimate in the CLM4.0 model as used in Meng et al. 2012. The average annual methane emissions were ~228 Tg/yr.

[3]CLM4.5 refers to the methane emissions estimated in CLM4.5 model. The estimated annual methane emissions from CLM4.5 were ~190 Tg/yr over the period of 1993-2004.

[3]GFED indicates the Global Fire Emission Database. Average annual CH4 emissions from GFED v2 and v3 are ~20 and ~21 Tg/yr, respectively.

[5]Wetland and rice paddies emissions from Ito and Inatomi (2012) were downscaled to approximately 183 Tg/yr over the period of 1993-2004 for TransCom.

CLM4.0 rice paddy emissions are 37 Tg/yr.

CLM4.5 rice paddy emissions are 42 Tg/yr.

Termite emissions from Fung et al. (1991) are 20 Tg/yr.

Note: The global total averaged emissions for the study period used in the TransCom, CN_a, and CN_b, BGC are the same (within 1% variation), but spatial distribution of methane emissions might be different.

Table 2 A list of stations used in this study.

Station #	Station Name	Lat	Lon	Elevation (m)	Data Availability
1	South Pole (spo)	-89.98	24.80W	2810	Feb.1983-Current
2	Cape Grim (cgo)	-40.68	144.68E	94	Jan. 1984-Current
3	Tutuila (Cape Matatula) (smo)	-14.24	170.57W	42	Apr. 1983-Current
4	Ascension Island (UK) (asc)	-7.92	14.42W	54	May.1983-Current
5	Cape Kumukahi (kum)	19.52	154.82W	3	Apr. 1983-Current
6	Mauna Loa (mlo)	19.54	155.58W	3397	May.1983-Current
7	Mt. Waliguan (wlg)	36.28	100.90E	3810	May.1991-Current
8	Tae-ahn Peninsula (tap)	36.72	126.12E	20	Mar.1993-Current
9	Niwot Ridge (nwr)	40.05	105.59W	3523	Jun.1983-Current
10	Mace Head (Ireland) (mhd)	53.33	9.90W	8	Jun.1991-Current
11	Cold Bay (cba)	55.2	162.72W	25	May.1983-Current
12	Barrow (brw)	71.32	156.60W	11	Jan.1986-Current
13	Zeppelinfjellet (Norway) (zep)	78.9	11.88E	475	May.1994-Current
14	Alert (Canada) (alt)	82.45	62.52W	210	Jun.1985-Current

Table 3. Comparison of the mean growth rate (ppb/yr) of atmospheric methane concentration in each simulation with observations

Station	lat	Obs	TransCom	CN_a	CN_b	BGC
spo	-89.98	4.61	6.11	5.05	3.62	6.44
cgo	-40.68	4.64	5.96	4.86	5.67	6.35
smo	-14.24	4.44	5.34	4.21	5.09	5.87
asc	-7.92	4.23	5.72	4.57	5.55	6.29
kum	19.52	3.75	4.21	3.37	4.12	5.46
mlo	19.53	3.95	4.37	3.46	4.28	5.59
wlg	36.28	4.39	4.3	3.27	4.37	6.34
tae	36.72	3.2	3.72	2.92	3.89	4.88
nwr	40.05	4.16	4.4	3.49	4.27	5.56
mhd	53.33	3.92	2.78	1.98	2.98	4.52
cba	55.20	3.77	3.97	3.31	3.81	6.2
brw	71.32	3.27	3.42	2.92	3.35	6.42
zep	78.90	3.42	0.92	-0.48	1.99	4.2
alt	82.45	4.6	3.67	3.08	3.65	5.47
Average		4.03	4.21	3.29	4.05	5.69

Table 4. Model performance statistics including the Root Mean Square Error (RMSE) and bias (ppb/yr). Bias is calculated as the absolute deviation of the mean between model simulations and observations.

	N-S Gradients	Growth Rate				Interannual Variability			
RMSE		South Pole	Mauna Loa	Niwot Ridge	Alert	South Pole	Mauna Loa	Niwot Ridge	Alert
TransCom	25.92	5.41	3.55	2.44	11.65	10.47	8.28	7.35	8.69
CN_a	17.57	0.57	4.22	2.88	5.13	12.65	13.96	14.59	15.06
CN_b	5.39	0.59	5.74	4.19	6.06	11.32	12.1	11.88	12.03
BGC	69.62	0.67	7.78	6.81	30.88	8.88	13.97	10.89	14.18
Bias		South Pole	Mauna Loa	Niwot Ridge	Alert	South Pole	Mauna Loa	Niwot Ridge	Alert
TransCom	0.26	0.58	0.3	0.22	-1.69	0.08	0.01	0.02	0.01
CN_a	0.17	0.03	0.05	0.29	-1.05	0.02	0.02	0.03	0.04
CN_b	0.02	0.07	0.06	0.34	-0.72	0.03	0.02	0.02	0.03
BGC	0.71	0.06	1.36	1.29	-3.13	0.01	0.02	0.02	0.04

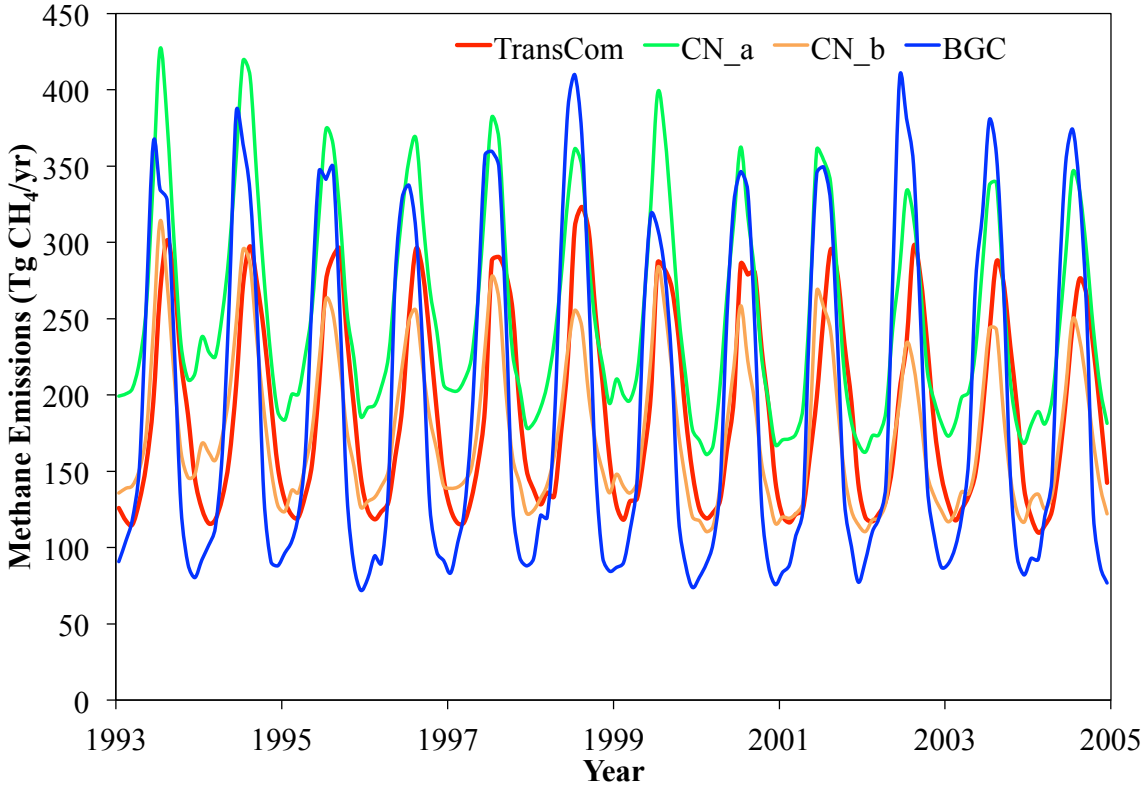

Fig. 1. Comparison of the time series of combined methane emissions from wetlands and rice paddies used in the TransCom (Patra et al. 2011), CN_a, CN_b, and BGC experiments. Note that the average methane budget over the period of 1993-2004 is the same in the TransCom, CN_a, CN_b, and BGC experiments. CN_b is the reduced CN_a.

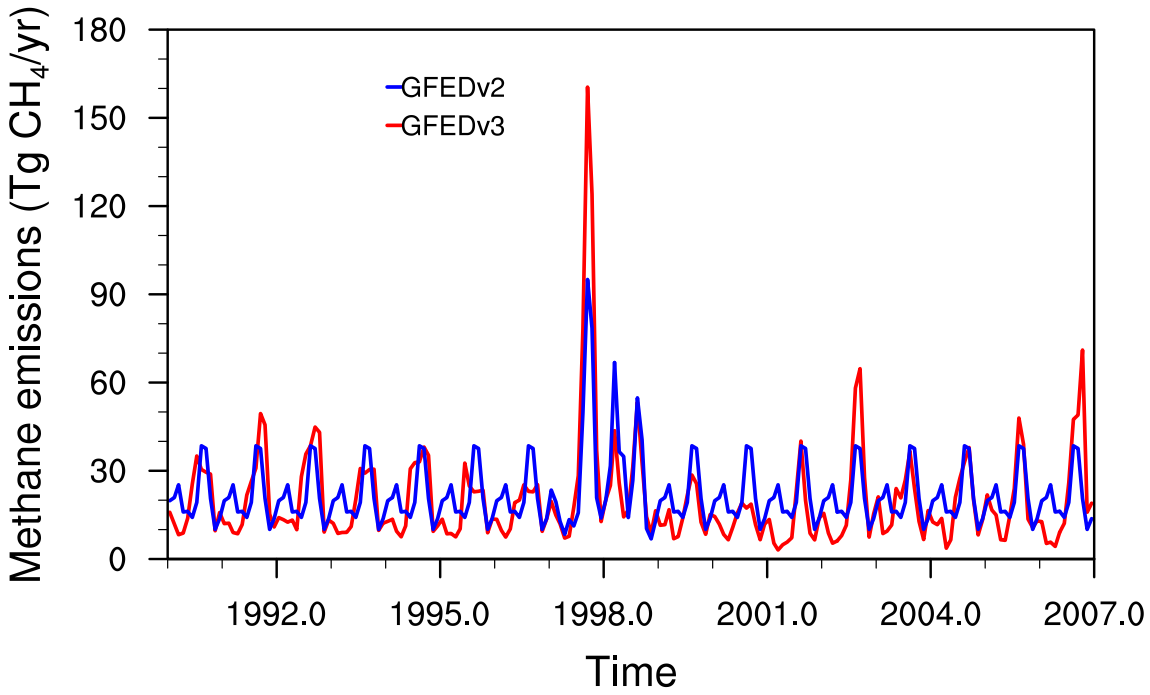

Fig. 2. Comparison of the inter-annual variation in methane emissions from fire in the GFED v2 (van De Werf et al., 1996) and GFED v3 (Gilglio et al., 2010). These datasets are obtained from http://www.globalfiredata.org/.

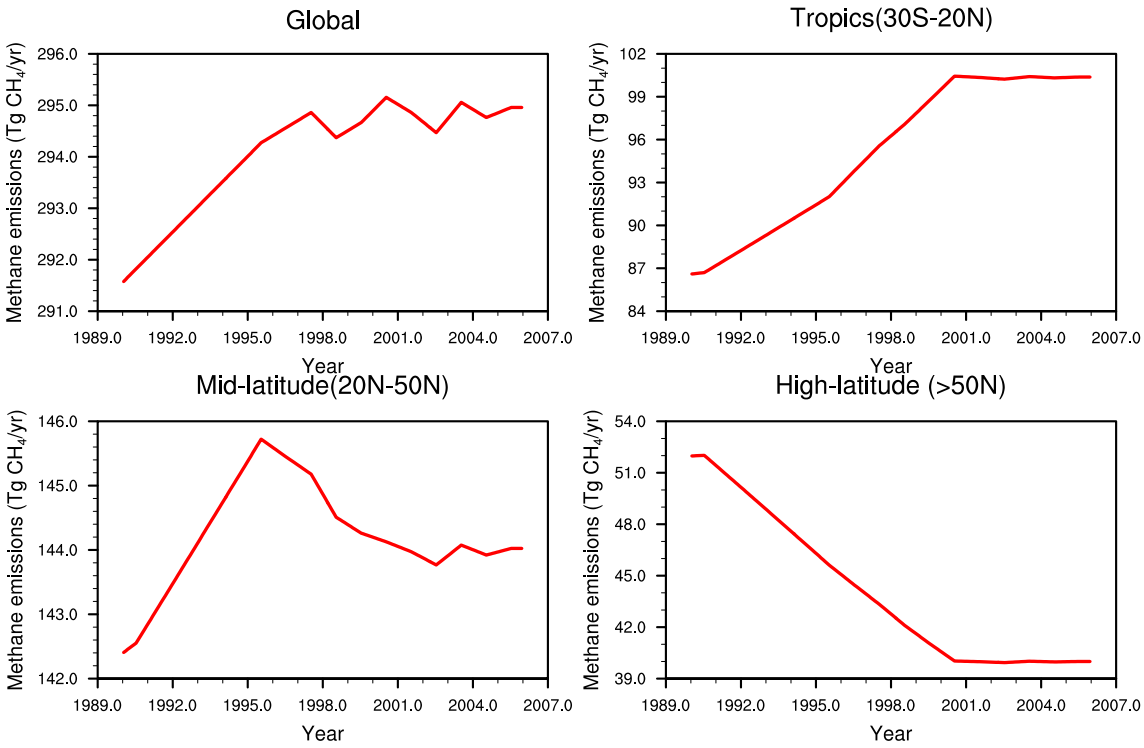

Fig. 3. The inter-annual anthropogenic methane emissions in the globe, tropics, mid-latitude, and high-latitude. These datasets are obtained from TransCom (Patra et al. 2010)

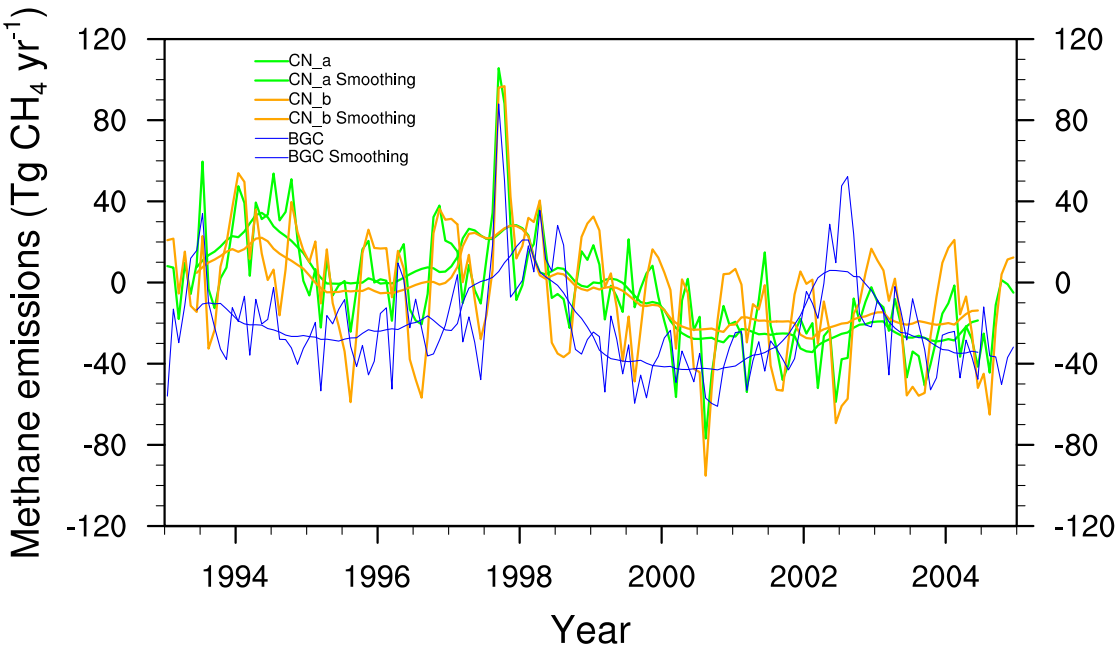

Fig. 4. The difference in total emissions used in CN_a, CN_b, BGC experiments as compared with TransCom. A 12-month smoothing is also plotted for the difference of CN_a (CN_a – TransCom), CN_b (CN_b – TransCom), BGC (BGC – TransCom) with TransCom. Please note that the average of the difference in the period of 1993-2004 is zero.

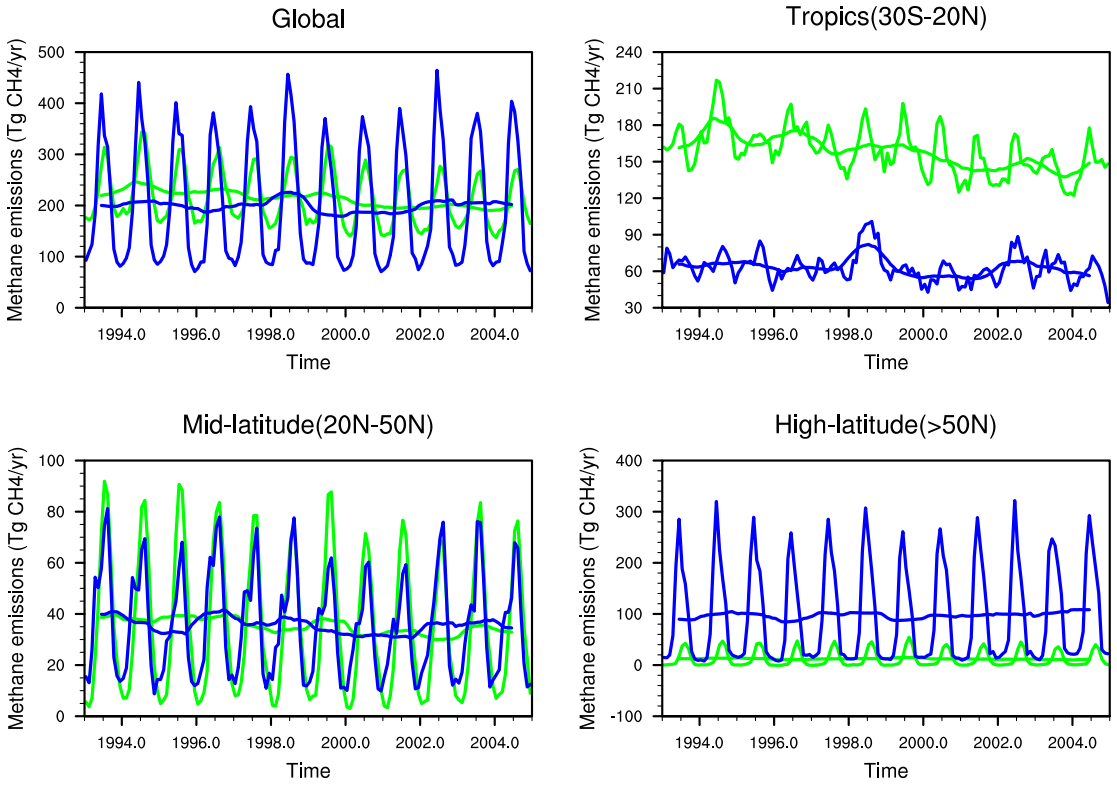

Fig. 5. Temporal variation of wetland CH_4 fluxes estimated in CN_a (green) and BGC (blue). The globe is divided into three regions: Tropics (30S-20N), Mid-latitude (20N-50N), and high-latitude (>50N). Please note that this is the original methane emissions produced by CN_a and BGC without any multiplication. The smooth green and blue lines indicate the 12-month average wetland CH_4 fluxes for CN_a and BGC.

A) CN_a

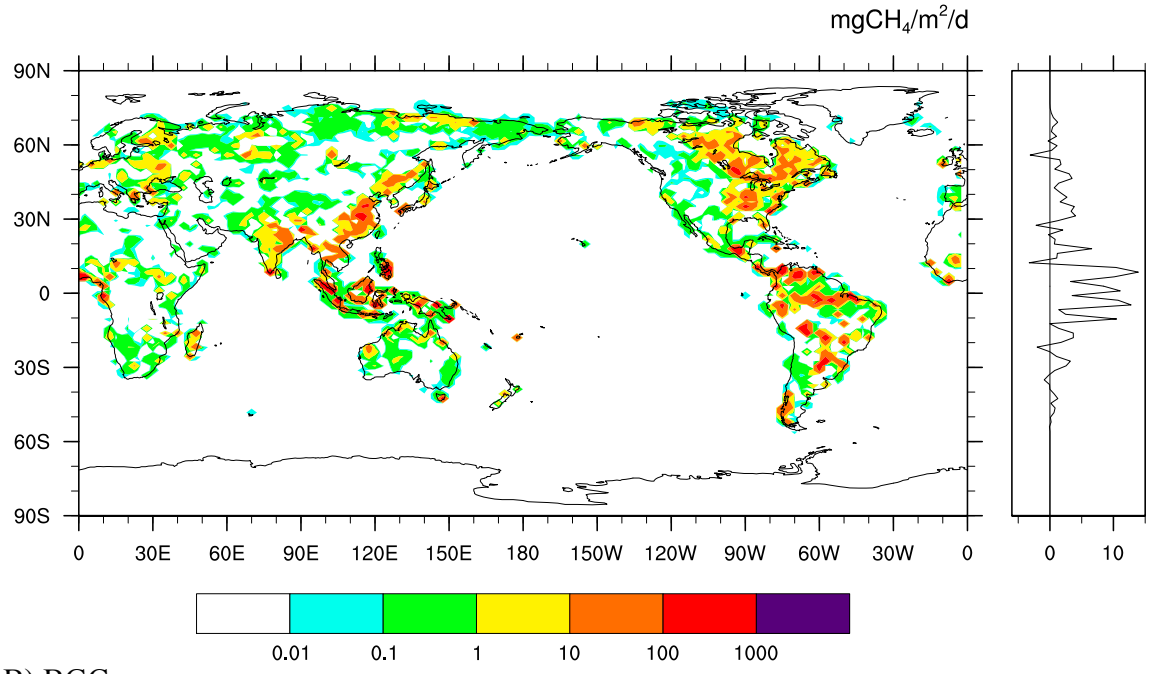

B) BGC

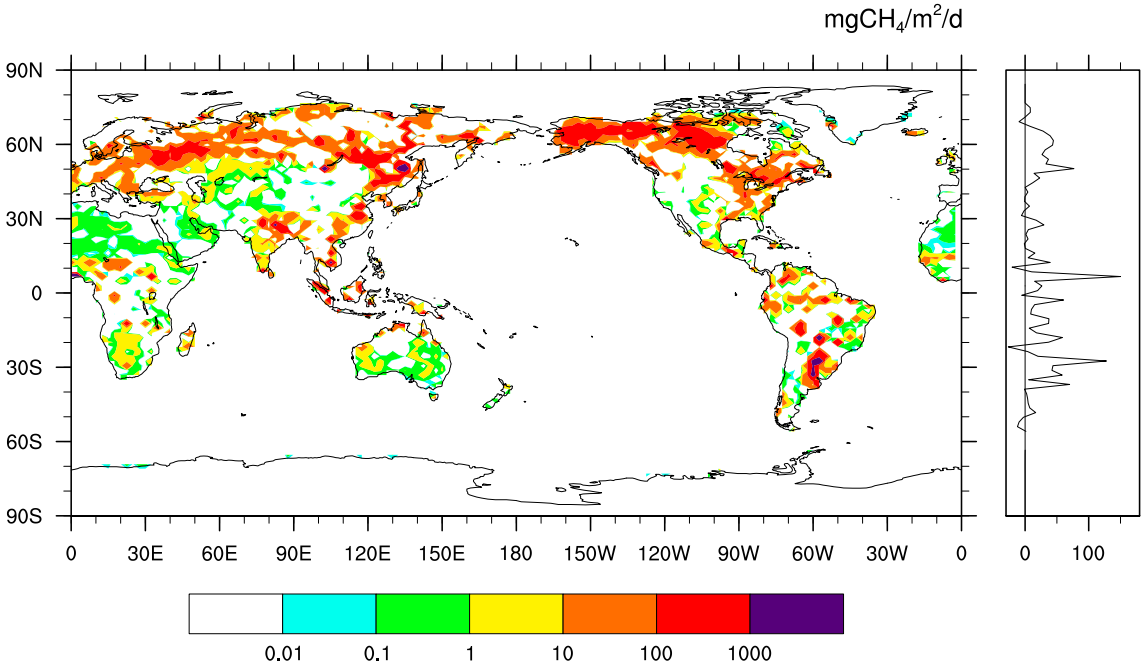

Fig. 6. The spatial difference in CH_4 fluxes between four high and low emission years. Please note CH_4 fluxes are plotted on a logarithmic color scale in CN_a (top, A) and BGC (bottom, B). The latitudinal average CH_4 flux is plotted on the right.

A) CN_a

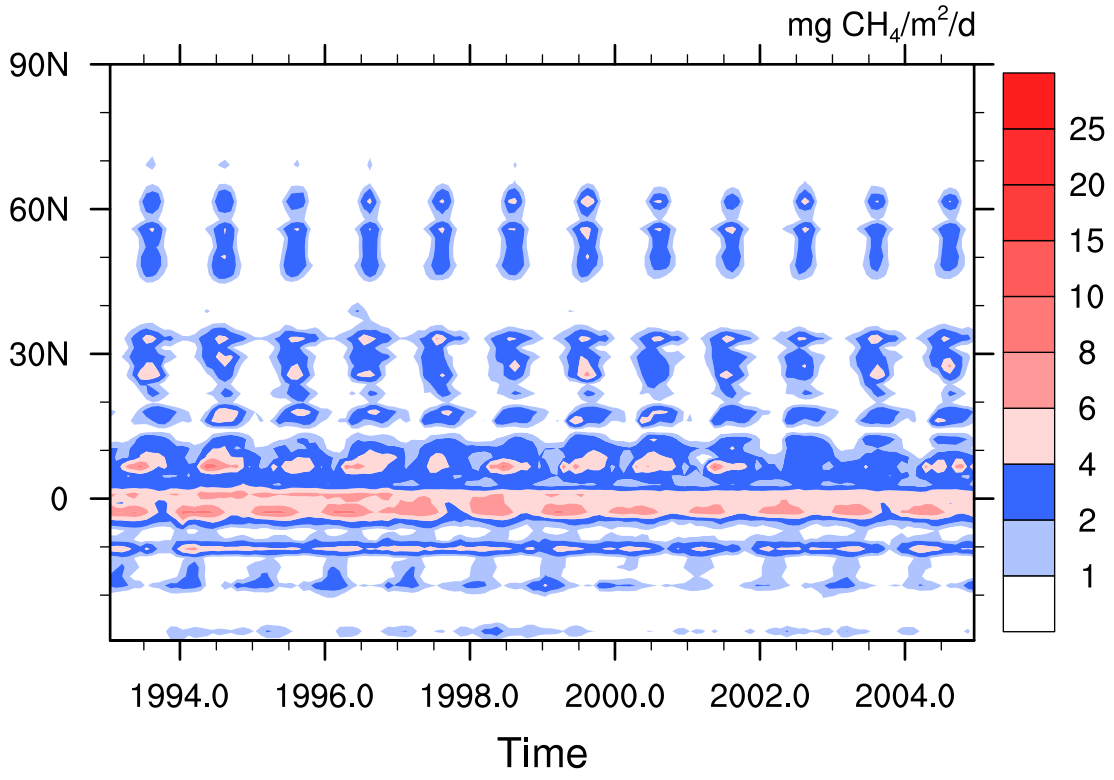

B) BGC

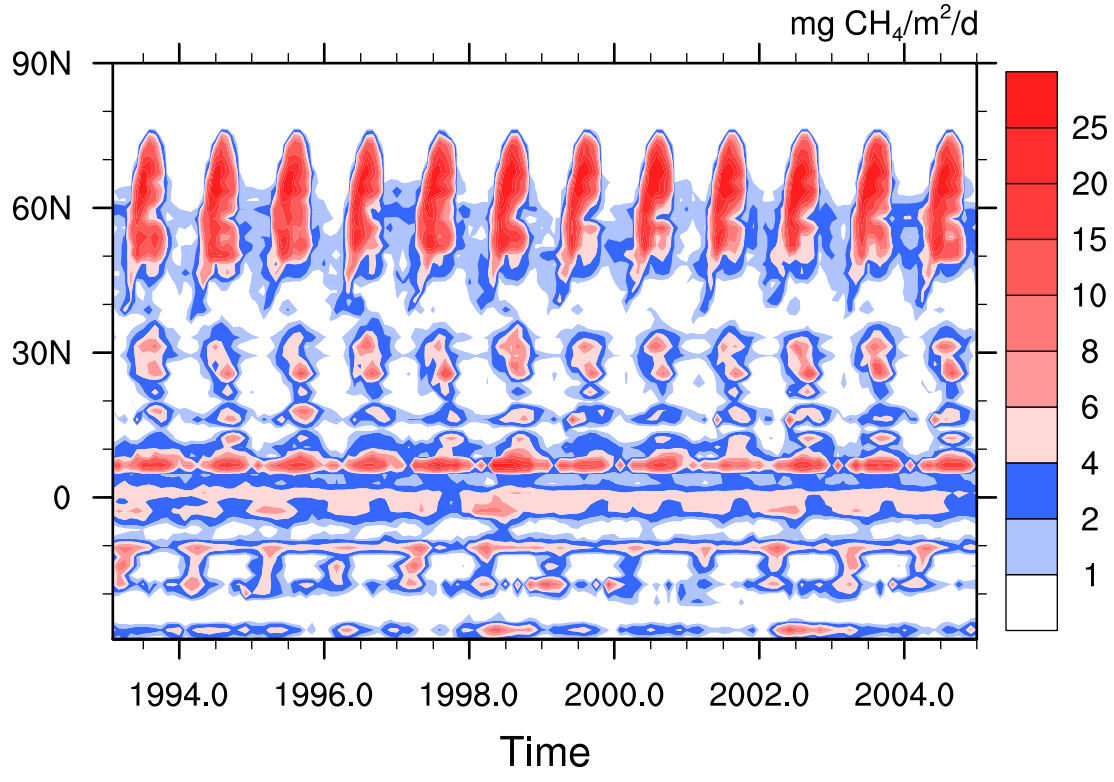

Fig. 7. Zonal average monthly methane fluxes with time in CN_a (top, A) and BGC (bottom, B) experiments.

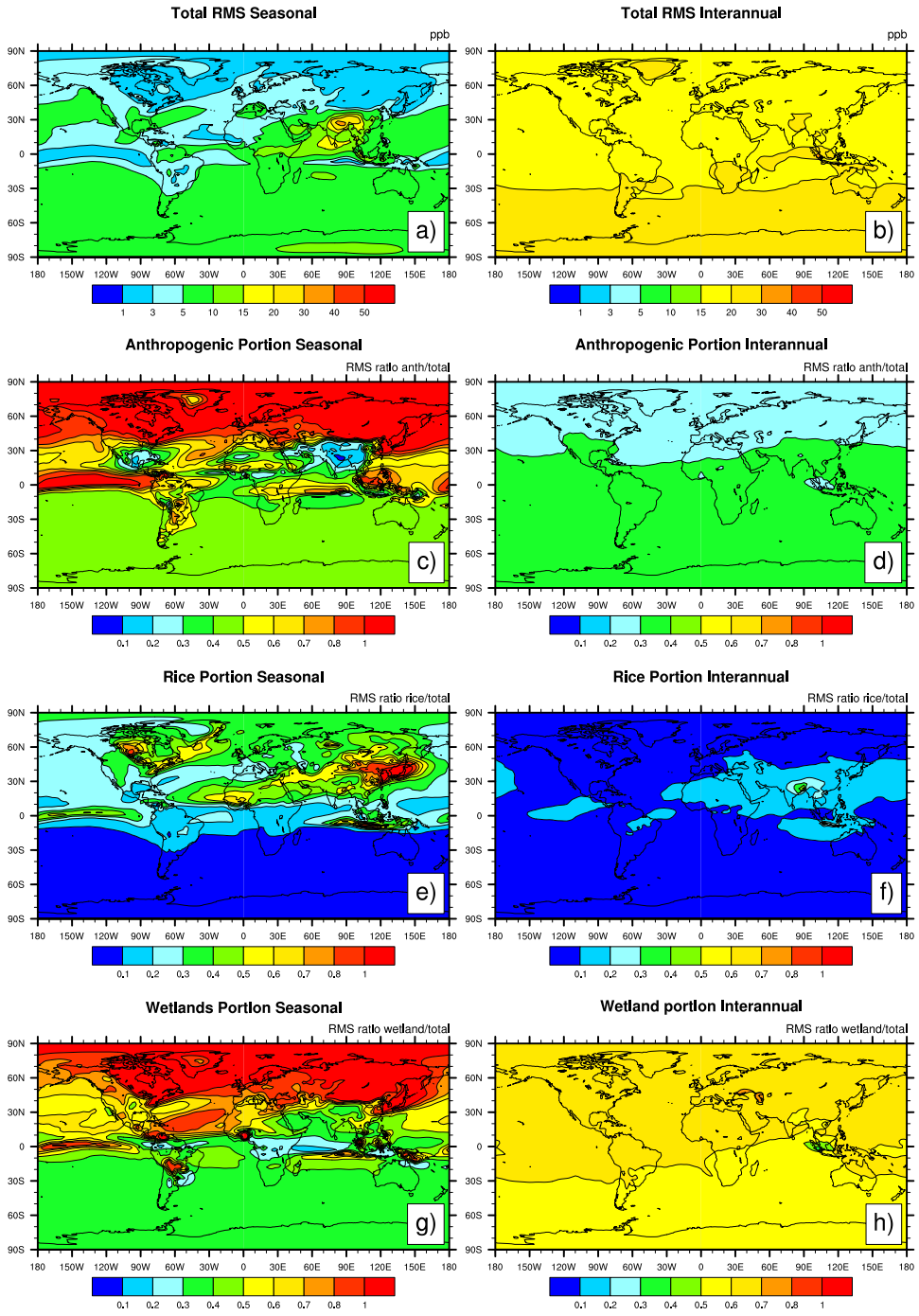

Fig. 8. RMS variability (in ppb) from 1993-2004 of atmospheric CH_4 concentration in CN_a experiment. The left panel shows seasonal RMS variability and the right panel indicates inter-annual RMS variability. From the top to the bottom are total RMS variability (a,b), anthropogenic contribution to total RMS variability (c,d), rice contribution to total RMS variability (e,f), and wetland contribution to RMS variability (g,h). Note that proportional RMS variability of anthropogenic sources, rice paddies, and wetlands add up to >1 when cancellation among component tracers occurs in the summing of total CH_4.

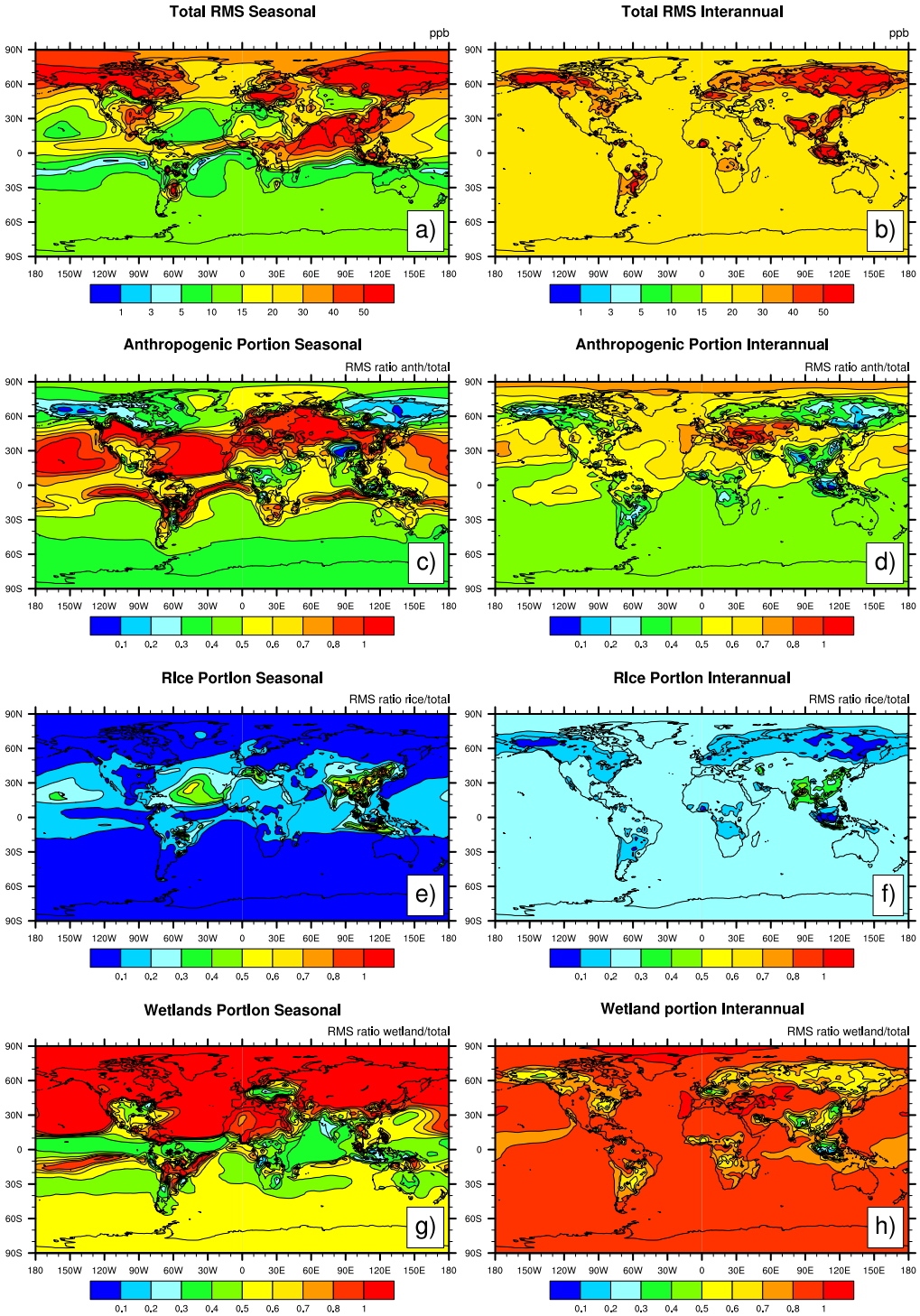

Fig. 9. RMS variability (in ppb) from 1993-2004 of atmospheric CH_4 concentration in BGC experiment. The left panel shows seasonal RMS variability and the right panel indicates inter-annual RMS variability. From the top to the bottom are total RMS variability (a,b), anthropogenic contribution to total RMS variability (c,d), rice contribution to total RMS variability (e,f), and wetland contribution to RMS variability (g,h). Note that portional RMS variability of anthropogenic sources, rice paddies, and

wetlands add up to >1 when cancellation among component tracers occurs in the summing of total CH_4.

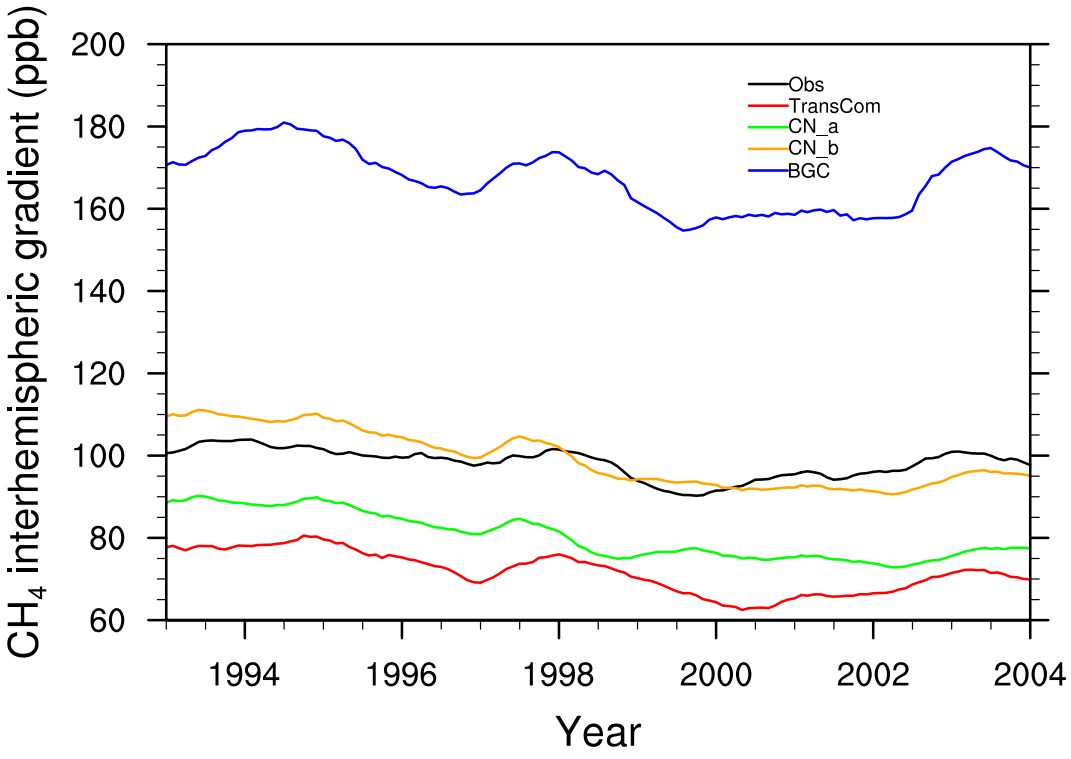

Fig. 10. The interhemispheric gradients (N-S) in atmospheric CH_4 concentration. The N-S gradients are calculated as the difference in atmospheric CH_4 concentration in Northern and Southern Hemispheres at these stations listed in Table 1. The observational CH_4 concentration dataset at these stations is from the World Data Centre for Greenhouse Gases (WDCGG) at http://ds.data.jma.go.jp/gmd/wdcgg/.

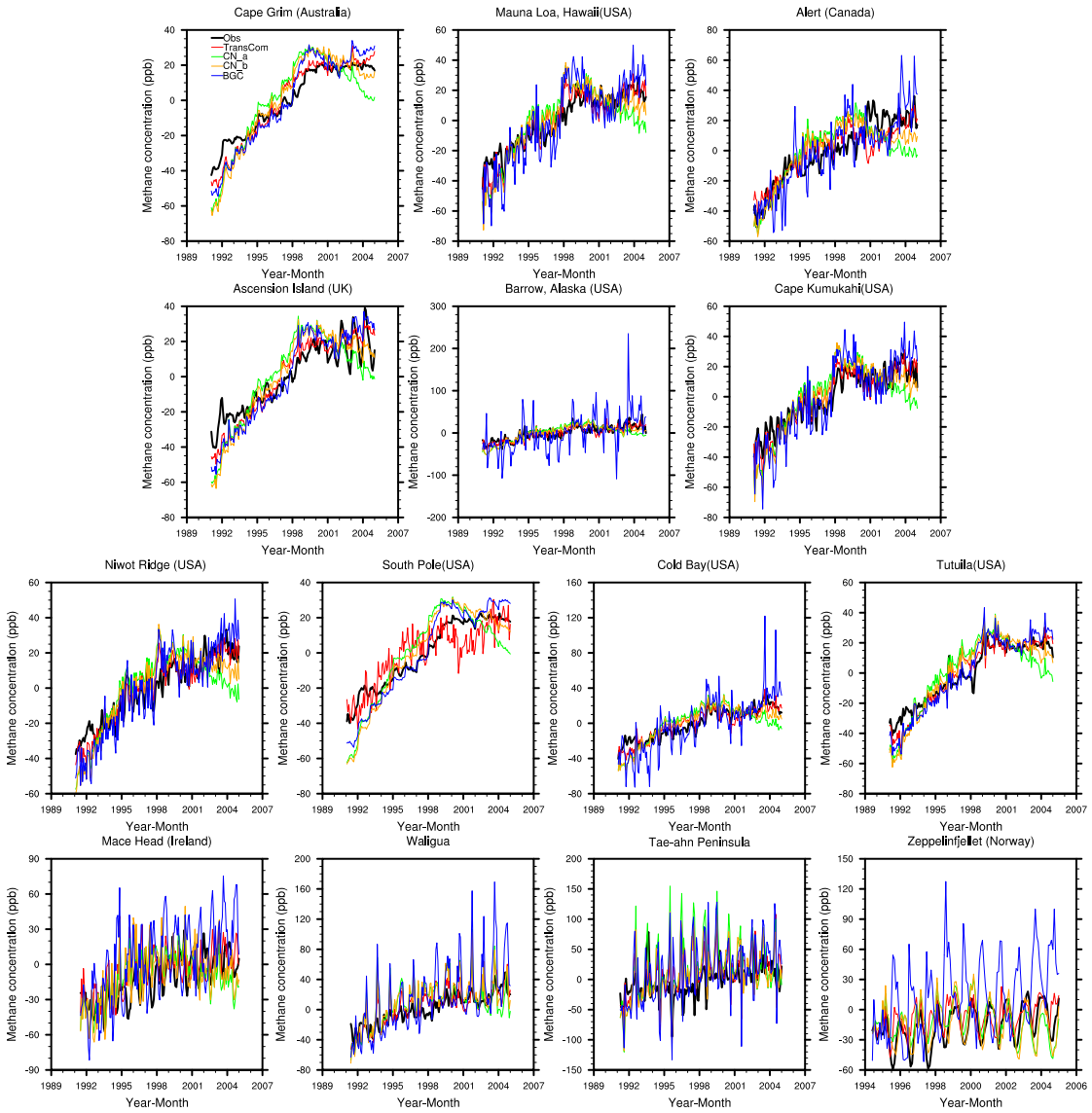

Fig. 11.The comparison of model simulated atmospheric CH4 concentration at closest grid box vs. observations. The climatological monthly mean is removed to focus on inter-annual variability in atmospheric CH_4 concentration at these stations. Model simulations are obtained from TransCom, CN_a, CN_b, and BGC experiments. The observational CH_4 concentration dataset at these stations is from the World Data Centre for Greenhouse Gases (WDCGG) at http://ds.data.jma.go.jp/gmd/wdcgg/.

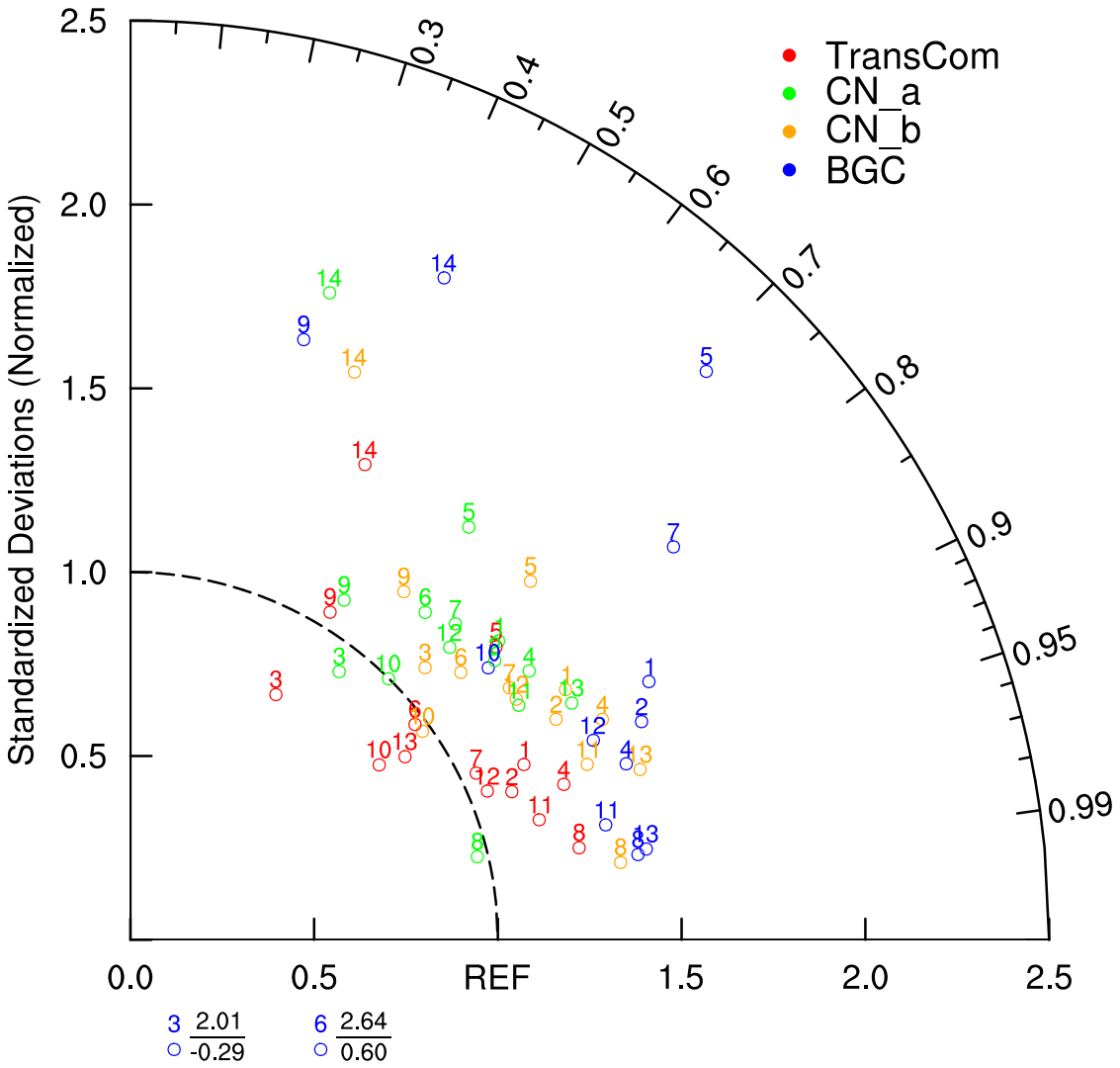

Fig. 12. Taylor diagrams comparing the model inter-annual variability to methane observations at 14 stations. In this Taylor diagram, the angel from the x-axis is the correlation coefficient between model and observed time series of atmospheric CH_4 concentration. The value on the radial axis is the ratio of standard deviation: $\sigma_{\text{model}}/\sigma_{\text{obs}}$. It represents the match between the amplitude of the model and observed inter-annual variability. Please refer to Table 2 for the stations associated with each number.

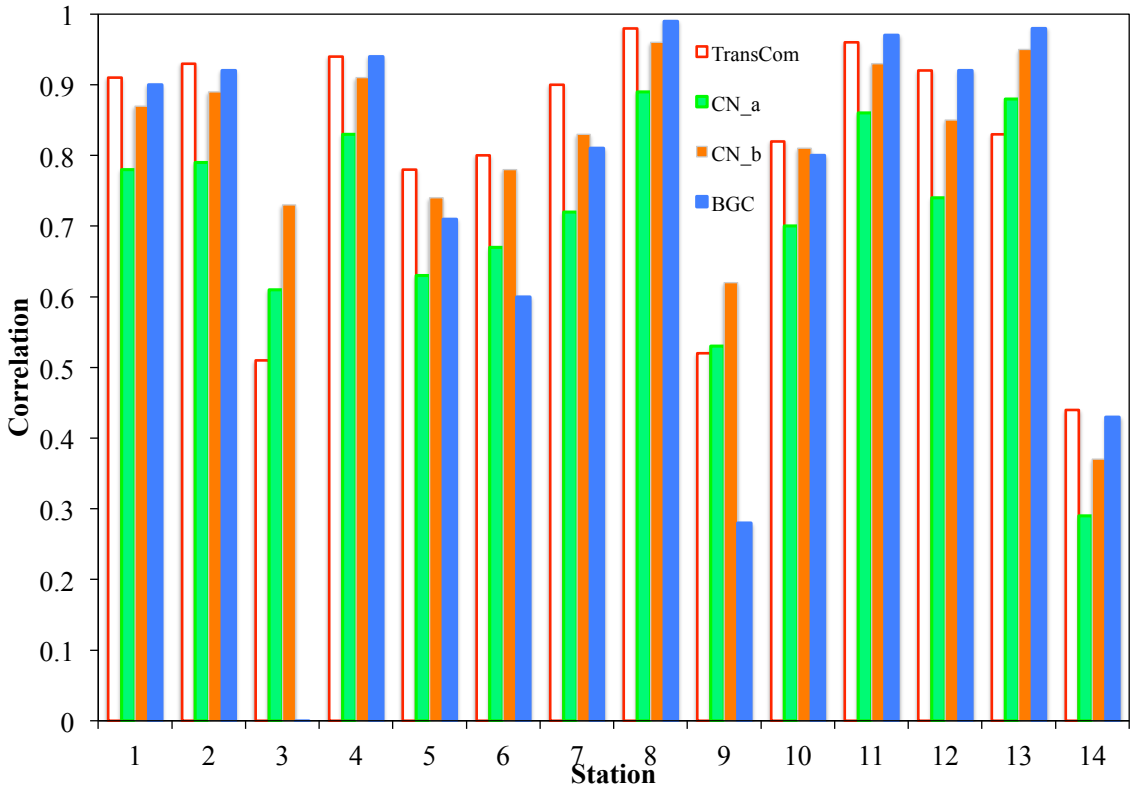

Fig. 13. Comparison of correlations between TransCom, CN_a, CN_b, BGC and observations (same as in Fig.12). The station # is corresponding to that in Table 2.

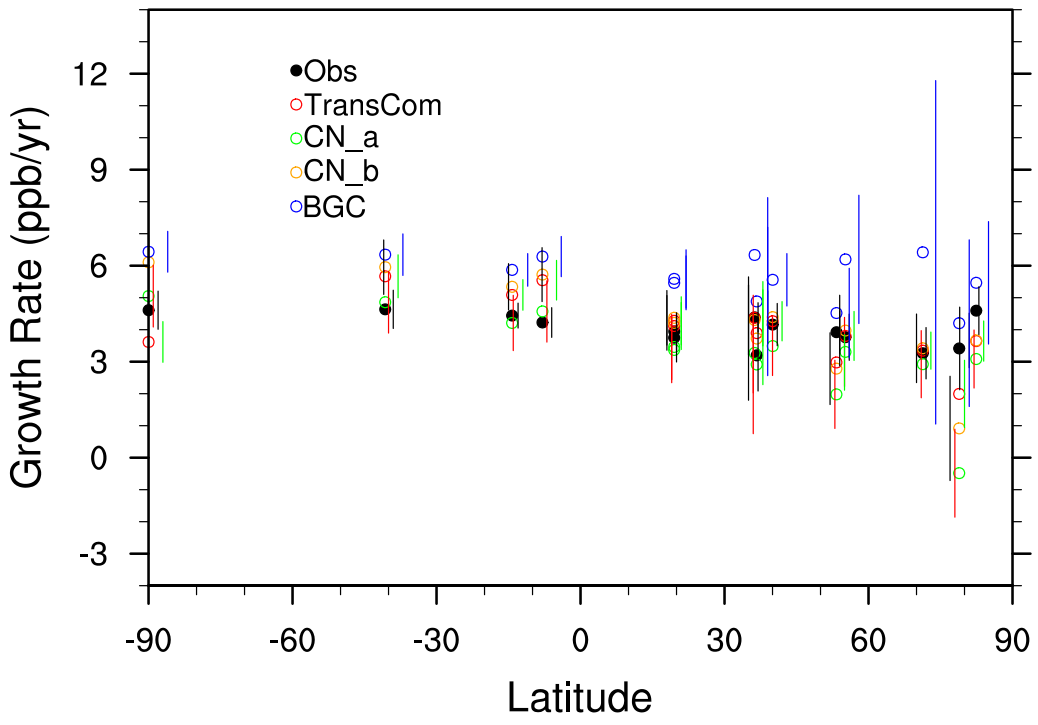

Fig. 14. Atmospheric CH_4 growth rate as a function of latitude in observations, TransCom, CN_a, CN_b, and BGC simulations. 90% confidence intervals are also shown.

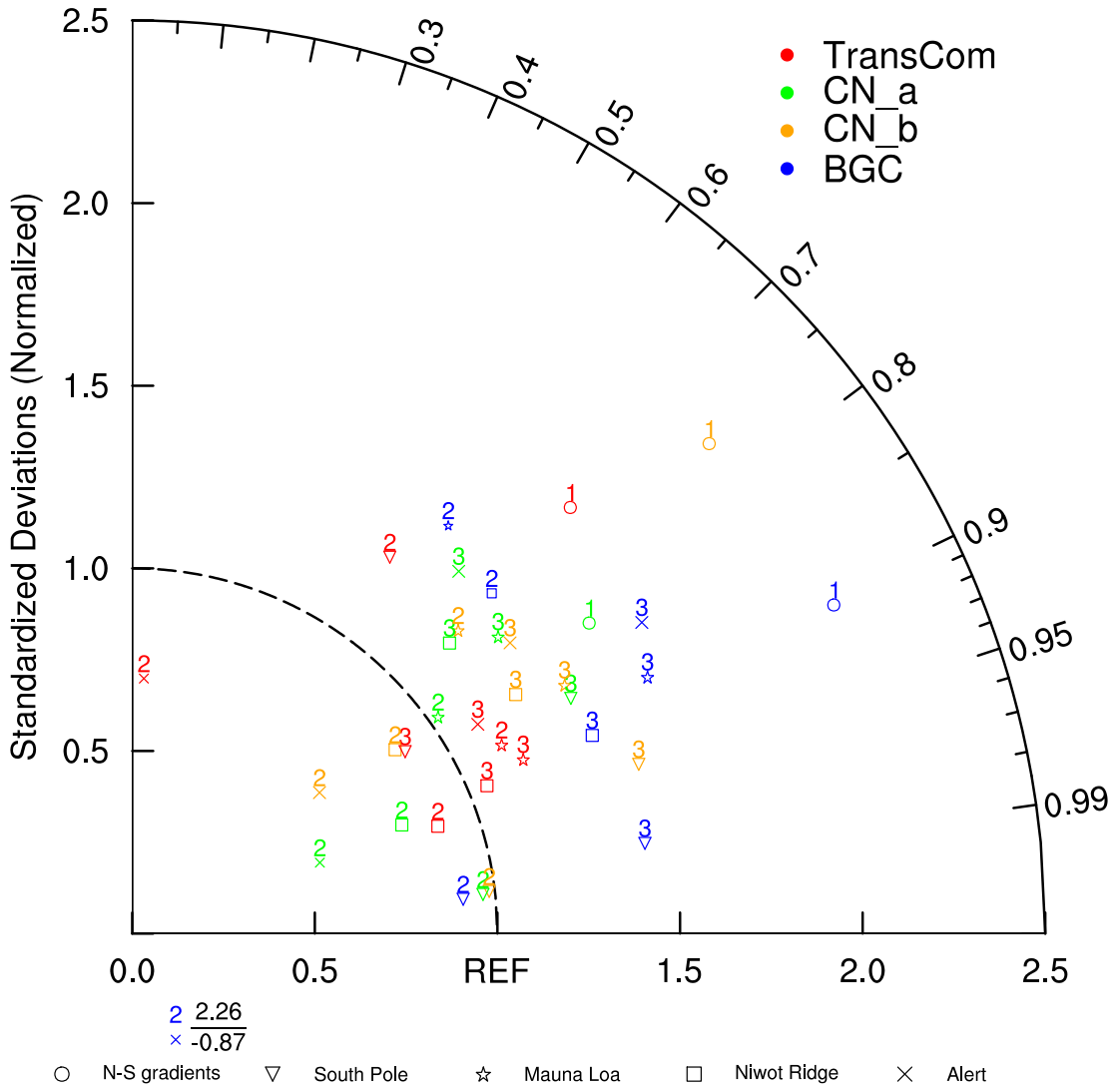

Fig. 15.Taylor diagram comparing model N-S gradients (#1), annual growth rates (#2), and interannual variability (#3) with observations for the South Pole, Mauna Loa, Niwot Ridge , and Alert (Canada) stations, respectively for the four simulations. The four stations are selected to represent the South Pole, tropics, mid-latitudes, and high latitudes. The annual growth rate is calculated as the difference between this year and previous year's mean methane concentration. The N-S gradients are from Fig. 10.

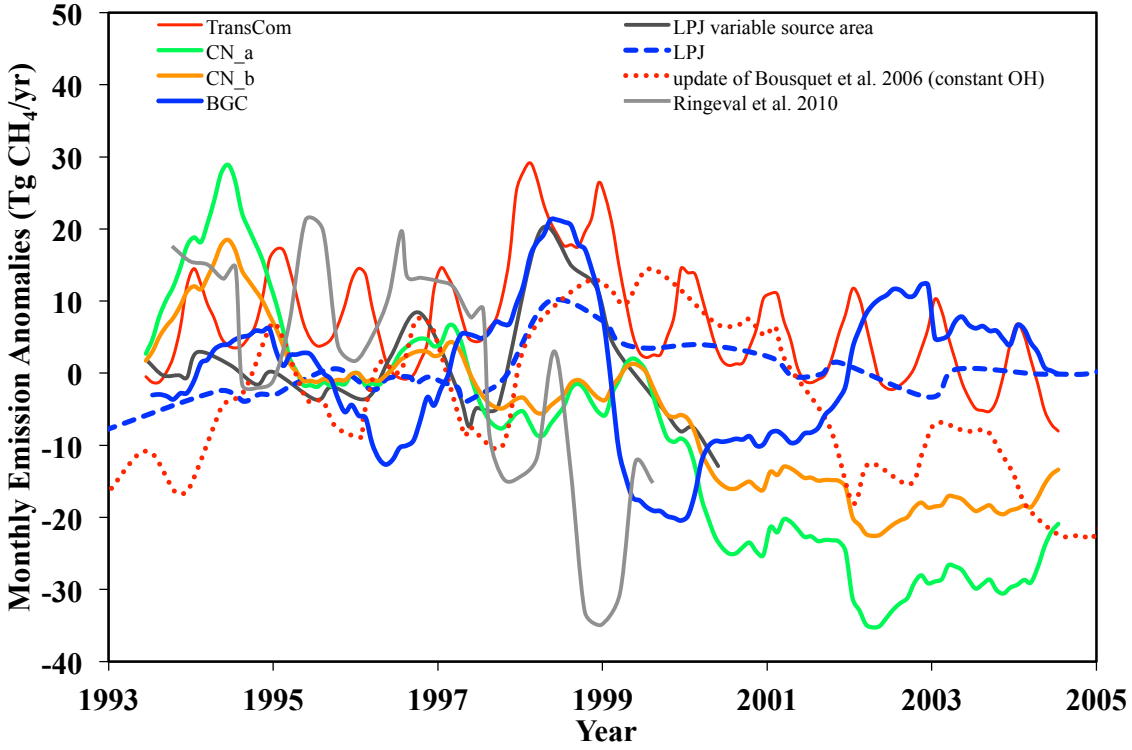

Fig. 16. Comparison of the inter-annual variability in wetland CH_4 emissions used in this study and in others. A centered 12-month running mean filter has been applied to smooth monthly output. Data for "LPJ variable source area", "LPJ", and "update of Bousquet et al. 2006 (constant OH)" are obtained from Spahni et al. 2011. "LPJ variable source area" indicates emissions anomalies for 1993-2000 calculated by using the observed monthly inundated area (Prigent et al. 2007). "LPJ" indicates global CH4 emission anomalies simulated by LPJ (natural ecosystem and rice agriculture) for scenario SC2 listed on Spahni et al. 2011. "update of Bousquet et al. 2006 (constant OH)" refers to global wetland emission anomalies derived from long-term atmospheric synthesis inversion updated from Bousquet et al. (2006). TransCom refers to emission anomalies derived from the combined wetland and rice paddies emissions. Methane emissions in Ringeval et al. (2010) are estimated using the ORCHIDEE global vegetation model with a process-based wetland CH4 emission model. The wetland area is prescribed to the observed monthly-inundated area (Prigent et al. 2007) in Ringeval et al. (2010). Please note that in this figure, "LPJ variable source area", "LPJ", and "update of Bousquet et al. 2006 (constant OH)" data are obtained from Spahni et al. 2011. The mean anomalies over 1993-2000 areadjusted to zero for the all data plotted on this graph.

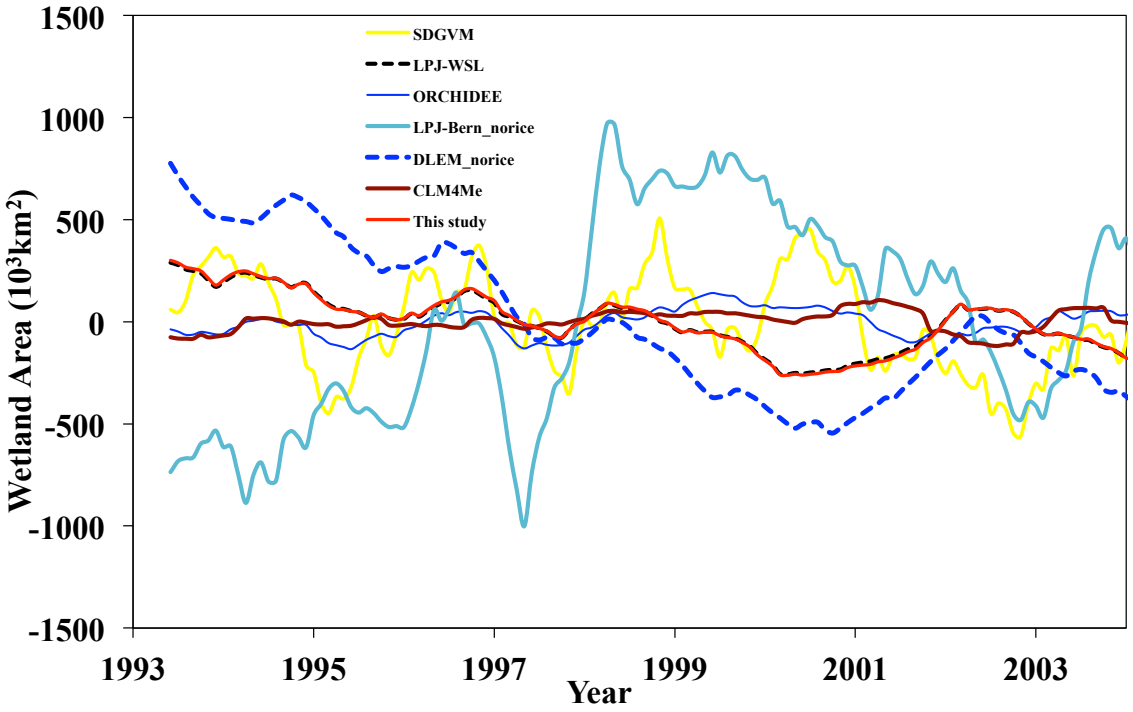

Fig. 17. 12-month smoothing of the anomalies in wetland areal extent used in the models that participate in WETCHIMP project (Melton et al. 2013; Wania et al. 2013) and in this study (satellite inundated area obtained from Prigent et al. 2007 and Papa et al. 2010). LPJ-Bern_norice and DLEM_norice are LPJ-Bern and DLEM models that do not include rice paddy simulations, respectively. These notifications indicate WETCHIP project also produce simulations with rice and only no rice simulations are included in this comparison study. In this figure, the long-term mean (1993-2004) is removed from each dataset.

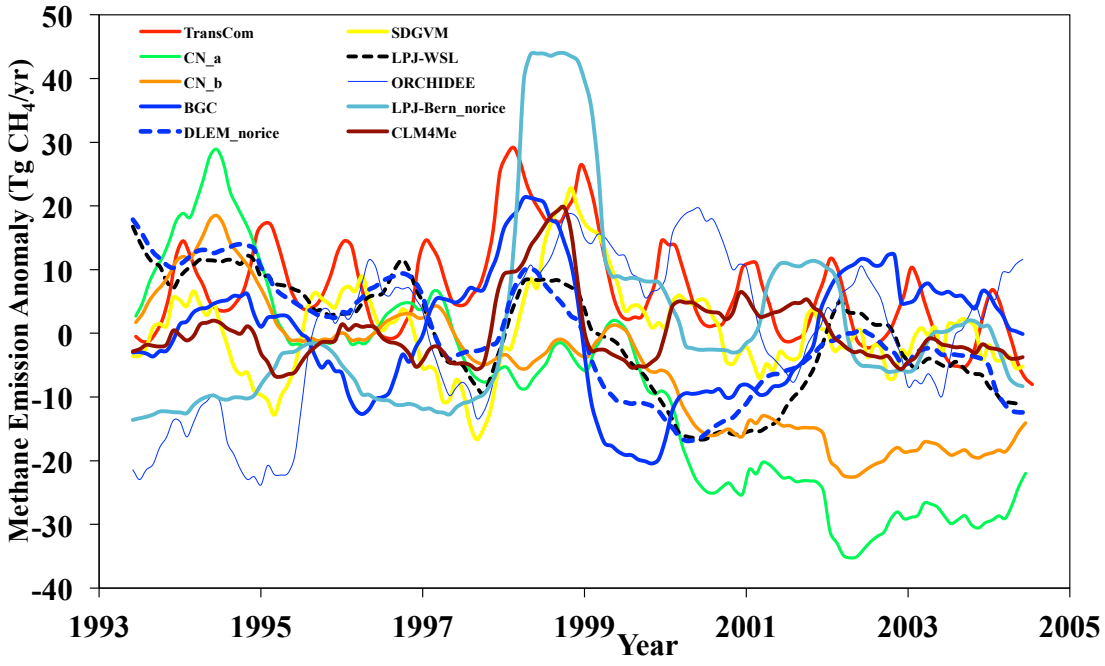

Fig. 18. Similar to Fig. 16, but for the models that participate in WETCHIMP (Melton et al. 2013; Wania et al. 2013). Each model uses a different wetland extent to estimate methane emissions (see Table 1 in Melton et al. 2013 for wetland determination scheme in each model). LPJ-WSL prescribes wetland area from monthly inundation dataset (Prigent et al. 2007, Papa et al. 2010). DLEM_norice prescribes the maximum wetland area from the inundation dataset with simulated intra-annual dynamics. SDVGM uses the internal hydrological model to determine wetland locations. All other models parameterize wetland areas based on inundation dataset or land cover dataset that produce different inter-annual and intra-annual variability in wetland area. Please also refer to Melton et al. (2013) for detailed description of each model (SDGVM, LPJ-WSL, ORCHIDEE, LPJ-Bern_norice, DLEM_norice, CLM4Me).

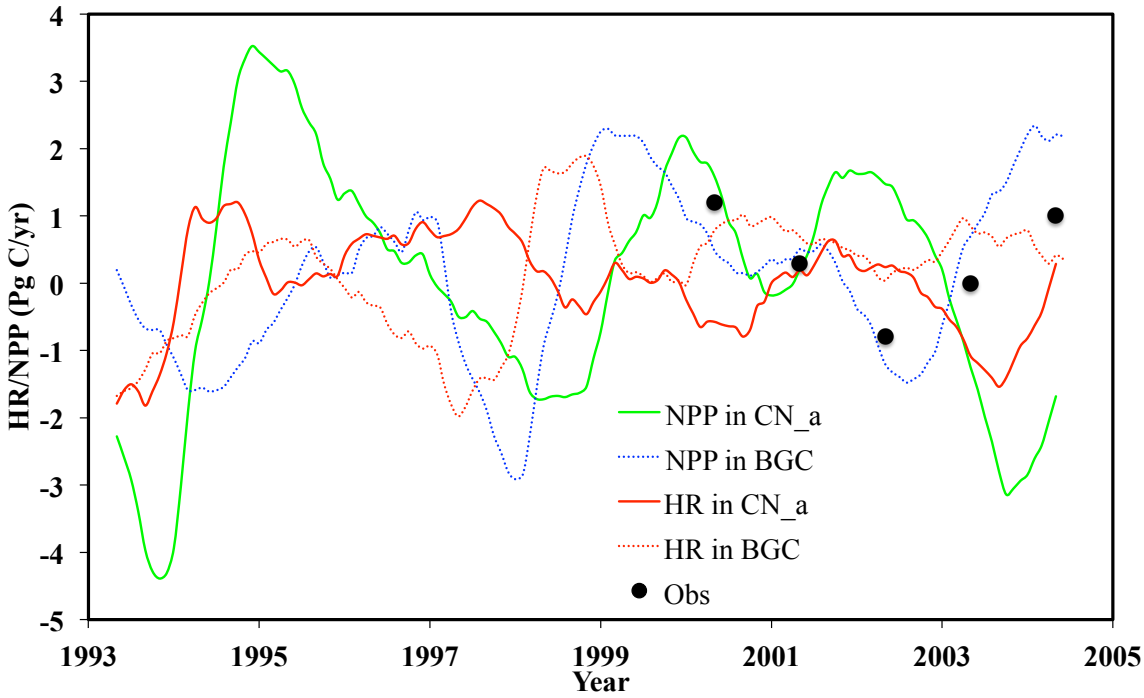

Fig. 19. Temporal variation of the anomalies in globally averaged heterotrophic respiration (HR) and net primary production (NPP) in CN_a and BGC experiments. Blue dots indicate globally averaged NPP anomalies from satellites obtained from Zhao and Running (Zhao and Running, 2010). A 12-month smoothing is applied to monthly anomalies in HR and NPP.

References

Bloom, A. A., Palmer, P. I., Fraser, A., Reay, D. S., and Frankenberg, C.: Large-Scale Controls of Methanogenesis Inferred from Methane and Gravity Spaceborne Data, Science, 327, 322-325, DOI 10.1126/science.1175176, 2010.

Bloom, A. A., Palmer, P. I., Fraser, A., and Reay, D. S.: Seasonal variability of tropical wetland CH4 emissions: the role of the methanogen-available carbon pool, Biogeosciences, 9, 2821-2830, 2012.

Bousquet, P., Ciais, P., Miller, J. B., Dlugokencky, E. J., Hauglustaine, D. A., Prigent, C., Van der Werf, G. R., Peylin, P., Brunke, E. G., Carouge, C., Langenfelds, R. L., Lathiere, J., Papa, F., Ramonet, M., Schmidt, M., Steele, L. P., Tyler, S. C., and White, J.: Contribution of anthropogenic and natural sources to atmospheric methane variability, Nature, 443, 439-443, Doi 10.1038/Nature05132, 2006.

Butler, J. H., Daube, B. C., Dutton, G. S., Elkins, J. W., Hall, B. D., Hurst, D. F., King, D. B., Kling, E. S., Lafleur, B. G., Lind, J., Lovitz, S., Mondeel, D. J., Montzka, S. A., Moore, F. L., Nance, J. D., Neu, J. L., Romashkin, P. R., Sheffer, A., and Snible, W. J.: Halocarbons and other atmospheric trace species., NOAA/US Department of Commerce, Boulder, Colorado, 115-135, 2004.

Chen, Y. H., and Prinn, R. G.: Estimation of atmospheric methane emissions between 1996 and 2001 using a three-dimensional global chemical transport model, Journal of Geophysical Research-Atmospheres, 111, D10307,doi:10310.11029/12005JD006058, 2006.

Cunnold, D. M., Steele, L. P., Fraser, P. J., Simmonds, P. G., Prinn, R. G., Weiss, R. F., Porter, L. W., O'Doherty, S., Langenfelds, R. L., Krummel, P. B., Wang, H. J., Emmons, L., Tie, X. X., and Dlugokencky, E. J.: In situ measurements of atmospheric methane at GAGE/AGAGE sites during 1985-2000 and resulting source inferences, Journal of Geophysical Research-Atmospheres, 107, 2002.

Denman, K. L., Brasseur, G., Chidthaisong, A., Ciais, P., Cox, P. M., Dickinson, R. E., Hauglustaine, D., Heinze, C., Holland, E., Jacob, D., Lohmann, U., Ramachandran, S., da Silva Dias, P. L., Wofsy, S. C., and Zhang, X.: Couplings Between Changes in the Climate System and Biogeochemistry. In: Climate Change 2007: The Physical Science Basis. Contribution of Working Group I to the Fourth Assessment Report of the Intergovernmental Panel on Climate Change [Solomon, S., D. Qin, M. Manning, Z. Chen, M. Marquis, K.B. Averyt, M.Tignor and H.L. Miller (eds.)]. Cambridge University Press, Cambridge, United Kingdom and New York, NY, USA, 2007.

Dlugokencky, E. J., Myers, R. C., Lang, P. M., Masarie, K. A., Crotwell, A. M., Thoning, K. W., Hall, B. D., Elkins, J. W., and Steele, L. P.: Conversion of NOAA atmospheric dry air CH4 mole fractions to a gravimetrically prepared standard scale, Journal of Geophysical Research-Atmospheres, 110, 2005.

Fung, I., John, J., Lerner, J., Matthews, E., Prather, M., Steele, L. P., and Fraser, P. J.: 3-Dimensional Model Synthesis of the Global Methane Cycle, Journal of Geophysical Research-Atmospheres, 96, 13033-13065, 1991.

Gent, P. R., Danabasoglu, G., Donner, L. J., Holland, M. M., Hunke, E. C., Jayne, S. R., Lawrence, D. M., Neale, R. B., Rasch, P. J., Vertenstein, M., Worley, P. H., Yang, Z. L.,

and Zhang, M. H.: The Community Climate System Model Version 4, Journal of Climate, 24, 4973-4991, 2011.
Giglio, L., Randerson, J. T., van der Werf, G. R., Kasibhatla, P. S., Collatz, G. J., Morton, D. C., and DeFries, R. S.: Assessing variability and long-term trends in burned area by merging multiple satellite fire products, Biogeosciences, 7, 1171-1186, 2010.
Ito, A., and Inatomi, M.: Use of a process-based model for assessing the methane budgets of global terrestrial ecosystems and evaluation of uncertainty, Biogeosciences, 9, 759-773, 2012.
Jauhiainen, J., Takahashi, H., Heikkinen, J. E. P., Martikainen, P. J., and Vasander, H.: Carbon fluxes from a tropical peat swamp forest floor, Global Change Biol, 11, 1788-1797, 2005.
Keller, M. M.: Biological sources and sinks of methane in tropical habitats and tropical atmospheric chemistry, PhD, Geological and Geophysical Sciences, Princeton University, 216 pp., 1990.
Kirschke, S., Bousquet, P., Ciais, P., Saunois, M., Canadell, J. G., Dlugokencky, E. J., Bergamaschi, P., Bergmann, D., Blake, D. R., Bruhwiler, L., Cameron-Smith, P., Castaldi, S., Chevallier, F., Feng, L., Fraser, A., Heimann, M., Hodson, E. L., Houweling, S., Josse, B., Fraser, P. J., Krummel, P. B., Lamarque, J. F., Langenfelds, R. L., Le Quere, C., Naik, V., O'Doherty, S., Palmer, P. I., Pison, I., Plummer, D., Poulter, B., Prinn, R. G., Rigby, M., Ringeval, B., Santini, M., Schmidt, M., Shindell, D. T., Simpson, I. J., Spahni, R., Steele, L. P., Strode, S. A., Sudo, K., Szopa, S., van der Werf, G. R., Voulgarakis, A., van Weele, M., Weiss, R. F., Williams, J. E., and Zeng, G.: Three decades of global methane sources and sinks, Nature Geoscience, 6, 813-823, 2013.
Kistler, R., Kalnay, E., Collins, W., Saha, S., White, G., Woollen, J., Chelliah, M., Ebisuzaki, W., Kanamitsu, M., Kousky, V., van den Dool, H., Jenne, R., and Fiorino, M.: The NCEP-NCAR 50-year reanalysis: Monthly means CD-ROM and documentation, Bulletin of the American Meteorological Society, 82, 247-267, 2001.
Koven, C. D., Riley, W. J., Subin, Z. M., Tang, J. Y., Torn, M. S., Collins, W. D., Bonan, G. B., Lawrence, D. M., and Swenson, S. C.: The effect of vertically resolved soil biogeochemistry and alternate soil C and N models on C dynamics of CLM4, Biogeosciences, 10, 7109-7131, 2013.
Lamarque, J. F., Emmons, L. K., Hess, P. G., Kinnison, D. E., Tilmes, S., Vitt, F., Heald, C. L., Holland, E. A., Lauritzen, P. H., Neu, J., Orlando, J. J., Rasch, P. J., and Tyndall, G. K.: CAM-chem: description and evaluation of interactive atmospheric chemistry in the Community Earth System Model, Geosci. Model Dev., 5, 369-411, doi:310.5194/gmd-5195-5369-2012, 2012.
Melton, J. R., Wania, R., Hodson, E. L., Poulter, B., Ringeval, B., Spahni, R., Bohn, T., Avis, C. A., Beerling, D. J., Chen, G., Eliseev, A. V., Denisov, S. N., Hopcroft, P. O., Lettenmaier, D. P., Riley, W. J., Singarayer, J. S., Subin, Z. M., Tian, H., Zurcher, S., Brovkin, V., van Bodegom, P. M., Kleinen, T., Yu, Z. C., and Kaplan, J. O.: Present state of global wetland extent and wetland methane modelling: conclusions from a model inter-comparison project (WETCHIMP), Biogeosciences, 10, 753-788, Doi 10.5194/Bg-10-753-2013, 2013.
Meng, L., Hess, P. G., Mahowald, N. M., Yavitt, J. B., Riley, W. J., Subin, Z. M., Lawrence, D. M., Swenson, S. C., Jauhiainen, J., and Fuka, D. R.: Sensitivity of wetland

1340 methane emissions to model assumptions: Application and model testing against site
1341 observations, Biogeosciences, 9, 2793-2819, doi:2710.5194/bg-2799-2793-2010, 2012.
1342 Mitchell, T. D., and Jones, P. D.: An improved method of constructing a database of
1343 monthly climate observations and associated high-resolution grids, International Journal
1344 of Climatology, 25, 693-712, 2005.
1345 Montzka, S. A., Krol, M., Dlugokencky, E., Hall, B., Jockel, P., and Lelieveld, J.: Small
1346 Interannual Variability of Global Atmospheric Hydroxyl, Science, 331, 67-69, Doi
1347 10.1126/Science.1197640, 2011.
1348 Olivier, J. G. J., and Berdowski, J. J. M.: Global emissions sources and sinks, in: The
1349 Climate System, edited by: Berdowski, J., Guicherit, R., and Heij, B.J., A.A.Balkema
1350 Publishers/Swets&Zeitlinger Pub., Lisse, The Netherlands, 2001.
1351 Papa, F., Prigent, C., Aires, F., Jimenez, C., Rossow, W. B., and Matthews, E.:
1352 Interannual variability of surface water extent at the global scale, 1993-2004, Journal of
1353 Geophysical Research-Atmospheres, 115, D12111, doi: 10.1029/2009JD012674, -, 2010.
1354 Patra, P. K., Houweling, S., Krol, M., Bousquet, P., Belikov, D., Bergmann, D., Bian, H.,
1355 Cameron-Smith, P., Chipperfield, M. P., Corbin, K., Fortems-Cheiney, A., Fraser, A.,
1356 Gloor, E., Hess, P., Ito, A., Kawa, S. R., Law, R. M., Loh, Z., Maksyutov, S., Meng, L.,
1357 Palmer, P. I., Prinn, R. G., Rigby, M., Saito, R., and Wilson, C.: TransCom model
1358 simulations of CH4 and related species: linking transport, surface flux and chemical loss
1359 with CH4 variability in the troposphere and lower stratosphere, Atmos Chem Phys, 11,
1360 12813-12837, 2011.
1361 Popova, Z., and Kercheva, M.: CERES model application for increasing preparedness to
1362 climate variability in agricultural planning - calibration and validation test, Phys Chem
1363 Earth, 30, 125-133, 2005.
1364 Prigent, C., Papa, F., Aires, F., Rossow, W. B., and Matthews, E.: Global inundation
1365 dynamics inferred from multiple satellite observations, 1993-2000, Journal of
1366 Geophysical Research-Atmospheres, 112, D12107,doi: 10.1029/2006JD007847, 2007.
1367 Qian, T. T., Dai, A., Trenberth, K. E., and Oleson, K. W.: Simulation of global land
1368 surface conditions from 1948 to 2004. Part I: Forcing data and evaluations, Journal of
1369 Hydrometeorology, 7, 953-975, 2006.
1370 Rigby, M., Prinn, R. G., Fraser, P. J., Simmonds, P. G., Langenfelds, R. L., Huang, J.,
1371 Cunnold, D. M., Steele, L. P., Krummel, P. B., Weiss, R. F., O'Doherty, S., Salameh, P.
1372 K., Wang, H. J., Harth, C. M., Mühle, J., and Porter, L. W.: Renewed growth of
1373 atmospheric methane, Geophy. Res. Letters, 35, L22805, doi: 10.1029/2008GL036037,
1374 2008.
1375 Riley, W. J., Subin, Z. M., Lawrence, D. M., Swenson, S. C., Torn, M. S., Meng, L.,
1376 Mahowald, N. M., and Hess, P. G.: Barries to predicting changes in global terrestrial
1377 methane fluxes: Analysis using CLM4ME, a methane biogeochemistry model integrated
1378 in CESM, Biogeosciences, 8, 1925-1953, doi: 1910.5194/bg-1928-1925-2011, 2011.
1379 Ringeval, B., de Noblet-Ducoudre, N., Ciais, P., Bousquet, P., Prigent, C., Papa, F., and
1380 Rossow, W. B.: An attempt to quantify the impact of changes in wetland extent on
1381 methane emissions on the seasonal and interannual time scales, Global Biogeochemical
1382 Cycles, 24, GB2003, doi: 10.1029/2008gb003354, 2010.
1383 Shannon, R. D., and White, J. R.: 3-Year Study of Controls on Methane Emissions from
1384 2 Michigan Peatlands, Biogeochemistry, 27, 35-60, 1994.

1385 Simmons, A. J., and Gibson, J. K.: The ERA-40 Project Plan. ERA-40 Project Report
1386 Series 1, 63 pp, 2000.
1387 Spahni, R., Wania, R., Neef, L., van Weele, M., Pison, I., Bousquet, P., Frankenberg, C.,
1388 Joos, F., Prentice, I. C., and van Velthoven, P.: Constraining global methane emissions
1389 and uptake by ecosystems, Biogeosciences, 8, 1643-1665,doi: 1610.5194/bgd-1648-
1390 1643-1665, 2011.
1391 Taylor, K. E.: Summarizing multiple aspects of model performance in a single diagram.,
1392 Journal of Geophysical Research-Atmospheres, 106, 7183-7192, 2001.
1393 Thornton, P. E., Lamarque, J. F., Rosenbloom, N. A., and Mahowald, N. M.: Influence of
1394 carbon-nitrogen cycle coupling on land model response to CO2 fertilization and climate
1395 variability, Global Biogeochemical Cycles, 21, Artn Gb4018
1396 Doi 10.1029/2006gb002868, 2007.
1397 Thornton, P. E., Doney, S. C., Lindsay, K., Moore, J. K., Mahowald, N., Randerson, J.
1398 T., Fung, I., Lamarque, J. F., Feddema, J. J., and Lee, Y. H.: Carbon-nitrogen interactions
1399 regulate climate-carbon cycle feedbacks: results from an atmosphere-ocean general
1400 circulation model, Biogeosciences, 6, 2099-2120, 2009.
1401 van der Werf, G. R., Randerson, J. T., Giglio, L., Collatz, G. J., Kasibhatla, P. S., and
1402 Arellano, A. F.: Interannual variability in global biomass burning emissions from 1997 to
1403 2004, Atmos Chem Phys, 6, 3423-3441, 2006.
1404 Wania, R., Melton, J. R., Hodson, E. L., Poulter, B., Ringeval, B., Spahni, R., Bohn, T.,
1405 Avis, C. A., Chen, G., Eliseev, A. V., Hopcroft, P. O., Riley, W. J., Subin, Z. M., Tian,
1406 H., van Bodegom, P. M., Kleinen, T., Yu, Z. C., Singarayer, J. S., Zurcher, S.,
1407 Lettenmaier, D. P., Beerling, D. J., Denisov, S. N., Prigent, C., Papa, F., and Kaplan, J.
1408 O.: Present state of global wetland extent and wetland methane modelling: methodology
1409 of a model inter-comparison project (WETCHIMP), Geosci Model Dev, 6, 617-641, Doi
1410 10.5194/Gmd-6-617-2013, 2013.
1411 Wuebbles, D. J., and Hayhoe, K.: Atmospheric methane and global change, Earth-Sci
1412 Rev, 57, 177-210, 2002.
1413 Xu, X. F., Tian, H. Q., Zhang, C., Liu, M. L., Ren, W., Chen, G. S., Lu, C. Q., and
1414 Bruhwiler, L.: Attribution of spatial and temporal variations in terrestrial methane flux
1415 over North America, Biogeosciences, 7, 3637-3655, 2010.
1416
1417